Superconvergent Cartesian Methods for Poisson type Equations in 2D–domains

Olivier Gallinato, Clair Poignard

Superconvergent Cartesian Methods for Poisson type Equations in 2D–domains

Olivier Gallinato, Clair Poignard

RESEARCH REPORT
N° 8809
November 2015
Project-Team MONC

ISSN 0249-6399 ISRN INRIA/RR--8809--FR+ENG

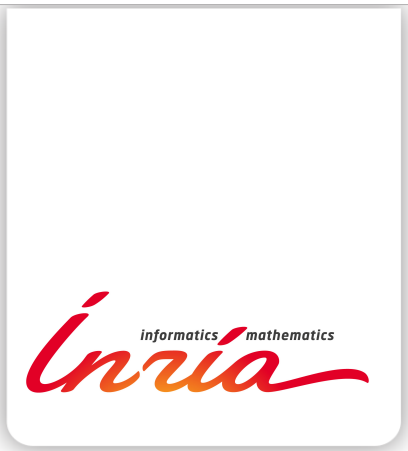

Superconvergent Cartesian Methods for Poisson type Equations in 2D–domains

Olivier Gallinato*, Clair Poignard*

Project-Team MONC

Research Report n° 8809 — November 2015 — 33 pages

Abstract: In this paper, we present three superconvergent Finite Difference methods on Cartesian grids for Poisson type equations with Dirichlet, Neumann or Robin conditions. Our methods are based on finite differences and high-order discretizations of the Laplace operator, to reach the superconvergence properties, in the sense that the first-order (and possibly the second-order) derivatives of the numerical solution are computed at the same order as the solution itself. We exhibit the numerical conditions that have to be fulfilled by the schemes to get such superconvergences and extensively illustrate our purpose by numerical simulations. We conclude by applying our method to a free boundary problem for cell protrusion formation recently proposed by the authors and colleagues. Note that quasistatic Stefan-like problem can be accurately solved by our methods.

Key-words: Finite differences on Cartesian grids, Superconvergence, Interface conditions, Free boundary problem
65M06, 65M12, 92C37

* Team MONC, INRIA Bordeaux-Sud-Ouest, Institut de Mathématiques de Bordeaux, CNRS UMR 5251 & Université de Bordeaux, 351 cours de la Libération, 33405 Talence Cedex, France.

RESEARCH CENTRE
BORDEAUX – SUD-OUEST

200 avenue de la Vieille Tour
33405 Talence Cedex

Méthodes de différences finies superconvergentes sur grille cartésienne pour les équations de Poisson dans des domaines bidimensionels

Résumé : Nous présentons 3 méthodes superconvergentes sur grilles cartésiennes pour des équations de Poisson avec condition de Dirichlet, Neumann ou Robin. Ces méthodes sont basées sur des différences finies et des discrétisation de l'opérateur de Laplace à un ordre élevé pour obtenir les propriétés de superconvergence. La superconvergence est au sens que les premières (et eventuellement secondes) dérivées d'une solution numérique sont au même ordre de précision que la solution elle-même. Nous proposons des conditions numériques auxquelles doivent satisfaire les schémas pour obtenir les propriétés de superconvergence, et nous illustrons de façon extensive notre proposition par des exemples numériques. Nous concluons en appliquant nos méthodes à un problèlme à frontière libre pour la formation de protrusion à l'échelle de la cellule, récemment proposés par les auteurs avec leurs collègues. Insistons sur le fait que le problème quasistatique de Stefan à 2 phases peut être calculé précisément par notre approche.

Mots-clés : Différences finies, Superconvergence, Conditions d'interface, Problème à frontière libre
65M06, 65M12, 92C37

Contents

1 Introduction

In this paper, we present three second order numerical methods on Cartesian grid for Poisson type equations in 2D-domains. The main insight of our methods lies in the *superconvergent* properties of the numerical solutions, in the sense that in addition to approximating the exact solution with a given order of accuracy (first or second), our methods makes it possible to approach they first-order (and even second order for the third method) derivatives with the same order of accuracy. We generically call *superconvergent* solutions the numerical solutions with such properties. Interestingly, our methods can handle Dirichlet, Neumann or Robin boundary conditions. They are based on finite differences and high-order discretizations of the Laplace operator, to reach the superconvergence properties.

It is usually assumed that the numerical gradient of a function has a truncation error of one order lower than the truncation error of the function itself. A superconvergent function contradicts that conjecture since, by definition, its gradient has a better accuracy than expected. Throuhout the paper, the concept of superconvergence must be understood as the same accuracy –or convergence rate– between a function and its gradient, in maximum norm. A superconvergent method is a method that produces a superconvergent solution under some assumptions on the data.

Several studies have addressed the superconvergence, especially for finite element type methods [16, 9, 1]. Regarding the finite difference methods, the available proofs of superconvergence generally consider the finite difference scheme as a special case of a finite element method, as in [6, 10]. In [6], Ferreira and Grigorieff have shown the gradient superconvergence in the case of general elliptic operators while Li *et al.* in [10] specifically studied the Shortley-Weller scheme and showed the second order superconvergence in the case of polygonal domains. In [11], Matsunaga and Yamamoto proved that the solution of the Shortley-Weller scheme was third order accurate near the interface, which can be seen as an essential aspect of the superconvergence property. The Shortley-Weller approximation, introduced in [13] in 1938, has been widely studied and is well-known for its gradient superconvergence property, without complete proof until very recently. More precisely, in [15], Yoon and Min proved the second order superconvergence in L^2-norm thanks to a discrete version of the divergence theorem, and Weynans, in [14], proposed a different proof for the maximum norm, involving analysis tools strongly inspired from Ciarlet [3]. Note that the available studies about superconvergent finite difference methods on domains are, to our knowledge, limited to cases with Dirichlet boundary conditions.

In [12] and [2], the authors numerically observed the superconvergence property for the variable coefficient Poisson equation, and on non-graded adaptive Cartesian grids. In the same numerical spirit, we present our superconvergent Cartesian methods that are built from the ghost-fluid method, introduced by Fedkiw *et al.* in [5]. Extrapolating the *ghost values* at different orders of accuracy result in different properties of superconvergence.

The domains that are considered are delimited by an interface, which is implicitly defined by the zero of a level set function. Using the ghost fluid method for the Laplace operator discretization consists of discretizing the second derivatives with the usual centered scheme and, if close to the interface, of extrapolating the *ghost value* at the point which is on the other side of the interface, from known values inside the integration area or on the boundary. The gradient and divergence operators, and the boundary conditions are computed with the same extrapolation order as for the Laplacian operator.

In this paper, we show that linear extrapolations give a second order method for the Dirichlet problem. Such a method has been proposed by Gibou *et al.* in [8], and it provides a first order superconvergent method for the Neumann or Robin conditions. Quadratic extrapolations give the Shortley-Weller scheme and, more generally, second order superconvergent methods for any of the 3 boundary conditions (Dirichlet, Neumann or Robin's type). Finally, cubic extrapolations provide a second order numerical method for which the solution has two levels of superconvergence: the numerical gradient and its numerical divergence are also second order accurate for any boundary conditions.

In contrast with the mathematical analyses mentioned above, our superconvergent results do not limit to the Dirichlet condition and do not require exact data. The novelty lies in the fact that for each of these methods, the superconvergence properties depend on the data accuracy (boundary data, second member of the equation and interface location). Some criteria on the minimal data accuracies that are required to preserve the superconvergence properties are numerically established. The main results are summarized in the final table 21. In particular, the two levels of superconvergence, on the gradient and its divergence, are preserved under

assumptions on data that are highly compatible with coupled problems.

One of the main motivations of the study, and probably the main result, lies in the need for methods that are well suited to coupled problems. In many free boundary problems, the interface velocity may depend on the gradient of a solution of another equation, for instance. This is particularly the case for 2-phase Stefan type problems and also in models for cell protrusion formations [7]. The superconvergence properties, and the relatively low requirements on data to reach them, make it possible to overcome an eventual loss of consistency due to this kind of coupling, or to get higher convergence rates.

After the presentation of the numerical schemes, we present the results of the accuracy tests throughout various test-cases. We then numerically establish criteria on the data accuracy and finally apply the methods and superconvergence properties to a dynamical coupled problem with moving interface.

2 General description of the methods to reach superconvergence properties

2.1 Statement of the problems

Throughout the paper, $\tilde{\mathcal{D}}$ is a domain of $\mathbb{R}^2$ and $\tilde{\mathcal{O}}$ is a connected domain strictly embbeded in $\tilde{\mathcal{D}}$, whose boundary is denoted by $\tilde{\Gamma}$, as depicted by Figure 1(a).

Given three data $\tilde{f}$ defined in $\tilde{\Omega}$, and $\tilde{g}$ and $\tilde{\rho}$ defined on $\tilde{\Gamma}$, we consider two problems satisfied by the generic solution $\tilde{u}$ in the domain generically denoted by $\tilde{\Omega}$:

- The Dirichlet problem:

$$\Delta\tilde{u} = \tilde{f}, \quad \text{in } \tilde{\Omega} := \tilde{\mathcal{O}}, \tag{1a}$$

$$\tilde{u} = \tilde{g}, \quad \text{on } \tilde{\Gamma}, \qquad \text{for the Dirichlet problem.} \tag{1b}$$

- The Robin problem

$$\Delta\tilde{u} = \tilde{f}, \quad \text{in } \tilde{\Omega} := \tilde{\mathcal{D}} \setminus \tilde{\mathcal{O}}, \tag{2a}$$

$$\partial_{\tilde{\mathbf{n}}}\tilde{u} + \tilde{\rho}\,\tilde{u} = \tilde{g}, \quad \text{on } \tilde{\Gamma}, \qquad \text{for the Robin problem,} \tag{2b}$$

$$u|_{\partial\tilde{\mathcal{D}}} = 0. \tag{2c}$$

Note that the Dirichlet condition on $\partial\tilde{\mathcal{D}}$ can be replaced by any other Robin or Neumann conditions. We only focus our interest on the interface $\tilde{\Gamma}$, which is described as the zero of a given level-set function $\tilde{\psi}$, and the domain of interest $\tilde{\Omega}$ is the location where $\tilde{\psi}$ is negative:

$$\tilde{\Gamma} = \left\{ x \in \mathbb{R}^2 : \quad \tilde{\psi}(x) = 0 \right\}, \quad \tilde{\Omega} = \left\{ x \in \mathbb{R}^2 : \quad \tilde{\psi}(x) < 0 \right\}.$$

Notation 1. *For the numerical resolution of the problem, the space is discretized with a Cartesian grid. The space step is denoted by h. Note that an accuracy at the order k has to be understood as an accuracy like $\mathcal{O}(h^k)$. Roughly speaking, letters with $\tilde{}$ refer to quantities in the continuous problem, and the same quantity in the discrete domain is denoted by the same letter without $\tilde{}$. More precisely, we use the following notations*

- *The numerical solution to problem* (1) *or to problem* (2) *is generically denoted by u.*

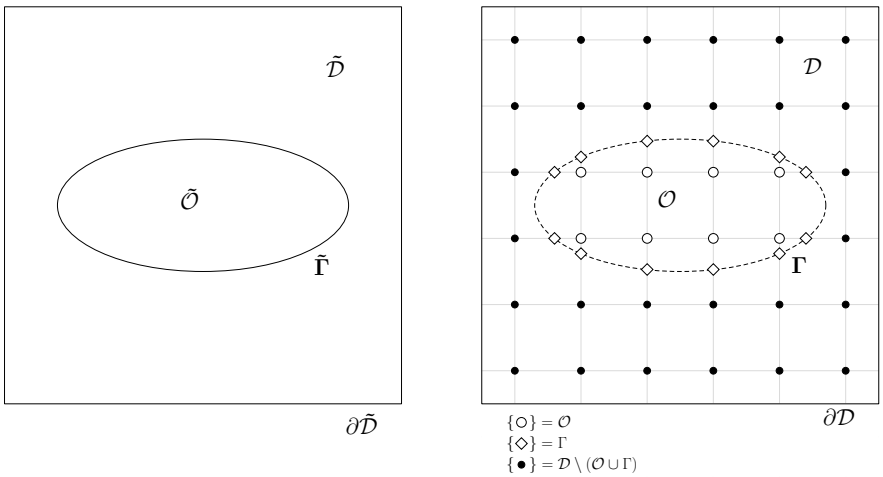

(a) geometry for the continuous problem

(b) discretized space for the numerical problem

Figure 1: Continuous and discrete representations of the geometry.

- *$\mathcal{D}$ denotes the set of grid points that belong to $\tilde{\mathcal{D}}$ and $\partial\mathcal{D}$ the set of intersections of $\partial\tilde{\mathcal{D}}$ with the grid axes,*
- *ψ is the restriction to $\mathcal{D}$ of the level set function $\tilde{\psi}$ or a discrete approximate of it, with a given order of accuracy,*
- *Ω is the set of points where ψ is negative. Note that it is the restriction of $\tilde{\Omega}$ to the grid only if ψ is the exact restriction of $\tilde{\psi}$,*
- *Γ is the set of points at the intersections of $\tilde{\Gamma}$ and the grid axes. Note that they rarely match with grid points. It is the restriction of $\tilde{\Gamma}$ to the grid axes only if ψ is the exact restriction of $\tilde{\psi}$,*
- *∇^h and Δ^h are the approximate operators of ∇ and Δ, with a given truncation error,*
- *∂_x^h and ∂_{xx}^h denote the numerical first and second x-derivatives respectively.*
- *φ is the exact or approximate restriction to Ω or Γ of any function $\tilde{\varphi}$ of $\tilde{\Omega}$ or $\tilde{\Gamma}$,*
- *φ_i denotes the value of any function φ at the point x_i on the considered axis. Throughout the presentation of the stencil, the point x_i is generically assumed to be in the domain of interest Ω, while x_{i-1} and x_{i+1} may or may not belong to Ω.*

Figure 1(b) summarizes geometric notations.

Note that the numerical operators are discretized direction by direction thanks to the ghost fluid method. In what follows, we just consider the x direction to describe the methods, as it is the same in the y direction. The *regular* points are the points of Ω whose neighbors, in the considered direction, are also in Ω. The points of Ω that have one neighbor at least which does not belong to Ω are considered to be close to the interface. The points of Γ are called interface points.

2.2 Discretization of the gradient and Laplace operators with the ghost fluid method

At the regular points of the grid, far from the interface, the first and second derivatives are computed at the order 2 with the usual centered schemes:

$$\partial_x^h u_i = \frac{u_{i+1} - u_{i-1}}{2\ h}, \tag{3}$$

$$\partial_{xx}^h u_i = \frac{u_{i+1} - 2\,u_i + u_{i-1}}{h^2}. \tag{4}$$

Close to the interface, either x_{i-1} or x_{i+1} is out[1] of Ω, where the solution u does not exist: the point x_{i-1} if the interface point u_Γ belongs to $[x_{i-1}, x_i]$, as in Figure 2, or the point x_{i+1} if u_Γ belongs to $[x_i, x_{i+1}]$. The value of the solution at this outer point is then called *ghost value* and

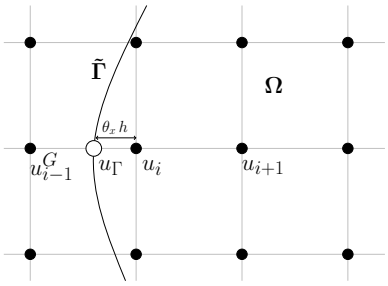

Figure 2: Ghost-Fluid method for the points near the interface.

has to be extrapolated from the existing values of the appropriate area. We consider two kinds of ghost values: the ghost values denoted by u_{i-1}^G (or u_{i+1}^G), that are extrapolated from solution values of Ω, for the gradient computation, and the ghost values denoted by $u_{i-1}^{G^\Gamma}$ (or $u_{i+1}^{G^\Gamma}$), that are extrapolated from the solution value on the neighboring interface point and from solution values of Ω, for the Laplacian computation. The first x-derivative of the solution u at the point x_i, in the example of Figure 2, is therefore discretized by

$$\partial_x^h u_i = \frac{u_{i+1} - u_{i-1}^G}{2\ h}, \tag{5}$$

where u_{i-1}^G denotes the ghost value which can be extrapolated from the values at the points x_i, x_{i+1}, x_{i+2}... The number of points used in the extrapolation depends on the order of the extrapolation. The second derivative is discretized by

$$\partial_{xx}^h u_i = \frac{u_{i+1} - 2\,u_i + u_{i-1}^{G^\Gamma}}{h^2}. \tag{6}$$

The specificity of the Laplace operator discretization lies in the use of the interface value, in order to take the boundary condition into account: the ghost value $u_{i-1}^{G^\Gamma}$ is extrapolated from the values at the points x_i, x_{i+1}... and x_Γ.
We consider three kinds of extrapolations for the ghost values: linear, quadratic and cubic extrapolations. In what follows, the corresponding schemes are referred to as L-scheme, Q-scheme and C-scheme, respectively.

[1]This is due to the fact that x_i is assumed to be in the domain Ω as explained in Notation.

2.3 Linear extrapolations and heuristic

In [8], Gibou *et al.* present a second order Cartesian method to compute the solution of the Dirichlet problem. The method is built with (4) at the regular points and (6) at the points close to the interface, using linear extrapolations for the ghost values. Let $\theta_x h$ denote the distance from the point of Γ to the closest point of Ω on the same x-axis, the ghost values are therefore given by

$$u_{i-1}^{G} = 2\,u_i - u_{i+1}, \tag{7}$$

$$u_{i-1}^{G^\Gamma} = \frac{1}{\theta_x}\,u_\Gamma - \frac{1-\theta_x}{\theta_x}\,u_i. \tag{8}$$

Then, close to the interface, the L-scheme reads

$$\partial_{xx}^h u_i = \frac{1}{\theta_x h^2}\,u_\Gamma - \frac{1+\theta_x}{\theta_x h^2}\,u_i + \frac{1}{h^2}\,u_{i+1}, \tag{9}$$

Note that if $\theta_x = 1$, the ghost point is coincident with the interface point and the scheme (9) is equivalent to (4). If $\theta_x = 0$, the point x_i is on the interface and does not belong to Ω. For now, the interface location –and therefore θ_x and θ_y– are assumed to be known exactly.
The authors of [8] emphasize the inconsistency of the second derivative near the interface, due to the linear extrapolation of the ghost value. However, they numerically highlight the second order accuracy of the method, despite this default of consistency.
Defining the gradient of the solution with (3) and (5), using the linear extrapolation (7) for the ghost values near the interface, we obtain the usual first order-derivative:

$$\partial_x^h u_i = \frac{u_{i+1} - u_i}{h}. \tag{10}$$

The gradient is therefore first order accurate in maximum norm –see results in Table 1 in section 3.1. However, restricting the error study to the center area, where the Laplace operator and the derivatives are consistent of order 2, the gradient error is then second order accurate in maximum norm (Table 2). It is consistent with the fact that the error is of order 2 in L^1-norm on the whole area Ω: the number of points, close to the interface, where the error of the gradient is not second order accurate is negligible for the discrete L^1-norm. Further restricting the area gives the same behavior for the error on the divergence of the gradient. These observations provide a heuristic: the superconvergence is related to the consistency of the Laplace operator, which justifies the use of higher extrapolation orders for ghost values to get superconvergence properties.

2.4 Quadratic and cubic extrapolations

The quadratic extrapolations of the ghost values are

$$u_{i-1}^{G} = 3\,u_i - 3\,u_{i+1} + u_{i+2}, \tag{11}$$

$$u_{i-1}^{G^\Gamma} = \frac{2}{\theta_x\,(1+\theta_x)}\,u_\Gamma - \frac{2\,(1-\theta_x)}{\theta_x}\,u_i + \frac{1-\theta_x}{1+\theta_x}\,u_{i+1}. \tag{12}$$

Then, the operator discretizations are given by

$$\partial_x^h u_i = \frac{-3\,u_i + 4\,u_{i+1} - u_{i+2}}{2\,h}, \tag{13}$$

$$\partial_{xx}^h u_i = \frac{2}{\theta_x\,(1+\theta_x)\,h^2}\,u_\Gamma - \frac{2}{\theta_x h^2}\,u_i + \frac{2}{(1+\theta_x)\,h^2}\,u_{i+1}, \tag{14}$$

which defines the Q-scheme. Since the ghost values are at the order 3, the discretizations of the first and second derivatives are second and first order accurate respectively. The scheme for the Laplace operator given by (4) at the regular points and (14) at the points close to the interface is the Shortley-Weller scheme [13].
The third method is built from cubic extrapolations, given by

$$u_{i-1}^{G} = 4\,u_i - 6\,u_{i+1} + 4\,u_{i+2} - u_{i+3}, \tag{15}$$

$$u_{i-1}^{G^\Gamma} = \frac{6}{\theta_x\,(1+\theta_x)\,(2+\theta_x)}\,u_\Gamma - \frac{3\,(1-\theta_x)}{\theta_x}\,u_i + \frac{3\,(1-\theta_x)}{1+\theta_x}\,u_{i+1} - \frac{1-\theta_x}{2+\theta_x}\,u_{i+2}, \tag{16}$$

and the operators of the C-scheme are defined by

$$\partial_x^h u_i = \frac{-4\,u_i + 7\,u_{i+1} - 4\,u_{i+2} + u_{i+3}}{2\,h}, \tag{17}$$

$$\partial_{xx}^h u_i = \frac{6}{\theta_x(1+\theta_x)(2+\theta_x)\,h^2}\,u_\Gamma - \frac{3-\theta_x}{\theta_x h^2}\,u_i + \frac{2\,(2-\theta_x)}{(1+\theta_x)\,h^2}\,u_{i+1} - \frac{1-\theta_x}{(2+\theta_x)\,h^2}\,u_{i+2}. \tag{18}$$

The fourth order ghost value (17) gives a second order first derivative, as for the quadratic case, due to the second order truncation error of the two-point centered stencil (5) of the derivative. As regards the Laplace operator, injecting the ghost value (16) in (6) gives a fully second order consistent operator. One can wonder why the cubic extrapolation is applied to compute the first derivative in this third method, since the quadratic extrapolation is sufficient to get the second order accuracy of the gradient. Once the solution computed, the computation of its *second derivative* must be understood as two successive numerical derivations using the operator ∂_x^h. Then, from the numerical point of view, the operator $\nabla^h \cdot \nabla^h$, which is the numerical divergence of the numerical gradient, is not the same as the numerical Laplace operator Δ^h. However, by construction of the operators, especially by construction of the numerical gradient from cubic extrapolations, we have the following property for any function $\tilde{\varphi}$ smooth enough:

$$\forall x_i \in \Omega, \qquad \nabla^h \cdot \nabla^h \varphi_i = \Delta^h \varphi_i + \mathcal{O}(h^2),$$

where φ is the restriction of $\tilde{\varphi}$ to the set Ω of grid points. This property seems to be essential to get the superconvergence on the numerical second derivative of the solution, that justifies the use of cubic extrapolations for both Laplace and gradient operators.
Finally, we have to mention the second member f of Equations (1a) and (2a). If approximated, it must preserve the Laplacian operator consistency at each point of the domain, regardless of the scheme. For the sake of simplicity, we consider that f is known on Ω with a second order of accuracy at least.

2.5 Boundary condition discretization

The interface value u_Γ is computed from the boundary condition before being injected in the desired scheme (9), (14) or (18), depending on the expected superconvergence properties. Obviously, the interface value computation also depends on the chosen scheme.

Dirichlet condition u_Γ is immediatly known if the boundary data g is given on the interface. However, in many problems, g may be given as the trace on the interface of an exterior scalar field, which may itself be approximated. A challenge of the study is to anticipate the nature of the approximation on this field to get the right superconvergence properties. In a first step,

we simply consider that the accuracy of the data must preserve that of the operator: g should be second order accurate to use the sceme (9) and to keep the zeroth order of consistency on the second derivative, near the interface. In the same way, it should be third order accurate to use (14) and fourth order accurate to use (18), in order to keep the first order and second order of consistency, respectively, of the operator near the interface. Thereby, the eventual given field and the extrapolations to get its trace on the interface should be at the same order of accuracy than the ghost values of the considered scheme. Actually, these assumptions about the boundary data, or the external field from which it is extrapolated, are too drastic and a refinement, mentioned in the introduction, is proposed in Section 4.1.

Neumann and Robin conditions The discretization of the Neumann or Robin condition involves the normal derivative on the interface, where the numerical operators are not defined. A second order method widely inspired from [4] is presented in [7] to handle the Neumann condition associated to the Shortley-Weller scheme, given by (4) and (14), for which the ghost value extrapolations are quadratic (Q-scheme). Interface operators ∂_x^Γ and ∂_y^Γ are introduced. They

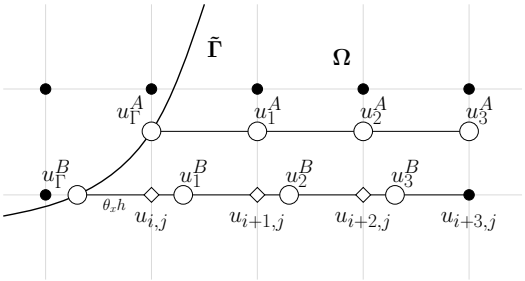

Figure 3: Interface derivative.

are directly or indirectly computed from other grid points, depending on wether the interface point belongs to the x-axis or y-axis. In the example of Figure 3, the point A is on the y-axis and the *indirect* x-derivative $\partial_x^\Gamma u_{\Gamma^h}^A$ is computed at order 2 from the sought value u_Γ^A, and the values u_1^A and u_2^A. To ensure the continuity in the stencil arrangement between both derivatives $\partial_x^\Gamma u_\Gamma^A$ and $\partial_x^\Gamma u_\Gamma^B$, the *direct* x-derivative $\partial_x^\Gamma u_\Gamma^B$ is computed in the same way from the value u_Γ^B, which is sought, and the values u_1^B and u_2^B. The interface derivatives are therefore discretized by

$$\partial_x^\Gamma u_\Gamma^A = \frac{-3\,u_\Gamma^A + 4\,u_1^A - u_2^A}{2\,h}, \tag{19}$$

$$\partial_x^\Gamma u_\Gamma^B = \frac{-3\,u_\Gamma^B + 4\,u_1^B - u_2^B}{2\,h}, \tag{20}$$

Then, u_1^B and u_2^B are quadratically interpolated from the values $u_{i,j}$, $u_{i+1,j}$ and $u_{i+2,j}$ while u_1^A and u_2^A are quadratically interpolated from the values of any neighboring grid points. To prevent these points from being on the other side of the interface, they are chosen in the direction of the corresponding ingoing normal component. For instance, in Figure 3, u_1^A is computed from the values $u_{i+1,j}$, $u_{i+1,j-1}$ and $u_{i+1,j-2}$. The Neumann/Robin condition is built in the same way for the L-scheme (9) and the C-scheme (18), just replacing the quadratic extrapolations by linear and cubic extrapolations, respectively. For the same configuration as in Figure 3, linear

extrapolations give the usual first order derivative:

$$\partial_x^\Gamma u_\Gamma^A = \frac{u_1^A - u_\Gamma^A}{h}, \tag{21}$$

$$\partial_x^\Gamma u_\Gamma^B = \frac{u_1^B - u_\Gamma^B}{h}, \tag{22}$$

and cubic extrapolations:

$$\partial_x^\Gamma u_\Gamma^A = \frac{-4\,u_\Gamma^A + 7\,u_1^A - 4\,u_2^A + u_3^A}{2\,h}, \tag{23}$$

$$\partial_x^\Gamma u_\Gamma^B = \frac{-4\,u_\Gamma^B + 7\,u_1^B - 4\,u_2^B + u_3^B}{2\,h}. \tag{24}$$

The values u_i^X are computed as described above, with the right order of extrapolation. Figure 4

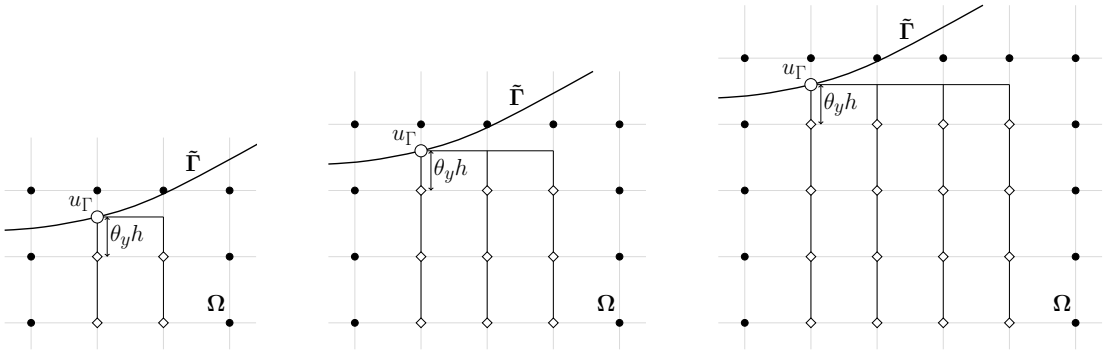

(a) linear extrapolations (b) quadratic extrapolations (c) cubic extrapolations

Figure 4: Examples of complete stencils for the interface normal derivative

gives examples of complete stencils for the interface normal derivative, which is therefore of the form

$$\partial_{\mathbf{n}}^\Gamma u_\Gamma = \frac{1}{2\,h}\left[\left(\alpha\,u_\Gamma + \sum_{i,j} a_{i,j}u_{i,j}\right) n_x^\Gamma + \left(\beta\,u_\Gamma + \sum_{i,j} b_{i,j}u_{i,j}\right) n_y^\Gamma\right], \tag{25}$$

where α, β, $(a_{i,j})$ and $(b_{i,j})$ are the known extrapolation parameters that depend on θ_x and θ_y. n_x^Γ and n_y^Γ are the components of the normal vector at the considered interface point. They are computed at each grid point with

$$\mathbf{n} = \frac{\nabla^h \psi_i}{|\nabla^h \psi_i|}, \tag{26}$$

thanks to the usual second order centered derivative of the level set function ψ, and the components on the interface are obtained with cubic interpolations. Then, the interface value of the solution is computed with (2b) and (25):

$$u_\Gamma = \frac{2\,h\,g - n_x^\Gamma \sum_{i,j} a_{i,j}u_{i,j} - n_y^\Gamma \sum_{i,j} b_{i,j}u_{i,j}}{\alpha\,n_x^\Gamma + \beta\,n_y^\Gamma + 2\,h\,\rho}, \tag{27}$$

and is injected in the discretization scheme of the Laplace operator. As for the Dirichlet condition, the boundary data g is taken at the same order than the ghost values of the considered scheme. A refinement, suggested by relation (27), one order below, is proposed in Section 4.1.

Importance of the stencil continuity to handle the Neumann/Robin condition Consider expressions (19) and (20), for instance. Developing (20) with quadratic extrapolations gives

$$\partial_x^\Gamma u_\Gamma^B = \frac{-3\,u_\Gamma^B + \frac{1}{2}\,\theta_x\,(5+3\,\theta_x)\,u_{i,j} - (3\,\theta_x^2 + 2\,\theta_x - 4)\,u_{i+1,j} - \frac{1}{2}\,(1-\theta_x)\,(2+3\,\theta_x)\,u_{i+2,j}}{2\,h}.$$

Thus, if θ_x tends to 0, both points x_Γ^A and x_Γ^B converge towards the point $x_{i,j}$ and both stencils of $\partial_x^\Gamma u_\Gamma^A$ and $\partial_x^\Gamma u_\Gamma^B$ tend to

$$\partial_x^\Gamma u_\Gamma = \frac{-3\,u_{i,j} + 4\,u_{i+1,j} - u_{i+2,j}}{2\,h},$$

which defines the continuity in the stencil arrangement. Note that using the interface derivative discretizations as in [4] is sufficient to achieve the numerical gradient superconvergence. However, one of the benefits of our approach lies in the fact that the interface unknowns that are needed by Cisternino *et al.* have not to be added in the discretization matrix. They are explicitely computed with (27) and injected in the scheme. Most of all, the continuous approach is absolutely required in the case of the use of the C-scheme, in order to achieve the superconvergence at the order 2 of $\nabla^h \cdot \nabla^h u$. Indeed, not ensuring the continuity of the stencils leads to jumps in the values of the numerical second derivative that prevent the superconvergence in maximum norm. For those reasons and for the sake of consistency between the methods, the continuous approach is systematically used for the Neumann and Robin problems.

2.6 Pathological configurations

In some configurations, which can be frequent in moving interface problems, there are not enough points on the same side of the interface to use the desired scheme, due to the local curvature. Some alternative discretizations are then required. We first consider the discretization of the Laplace operator. For instance, the configurations in Figure 5, at the point $x_{i,j}$, are pathological for the second x-derivative computation with the C-scheme, since the ghost value extrapolation requires four points in the x-direction. In Fig. 5(a), as they can be extrapolated only from one grid point and two interface points, the ghost values are extrapolated using grid points in the y-direction (circled points). In other more exotic configurations, as in Fig. 5(b), this is not possible. Then, the value $u_{i,j}$ is directly extrapolated from existing values of the solution (squared points).
Consider now the discretization of the boundary condition. The Dirichlet condition is not affected by these pathological configurations. As regards the Neumann condition, if the number of available points in one direction prevents the use of the appropriate discretization, we then use a scheme with a smaller stencil. For instance, the C-scheme needs 4 points for the discretization of the Neumann condition. If there are only 3, the discretization is done with that of the Q-scheme. If there are only 2, the discretization is done with that of the L-scheme.
Obviously, these patches may imply the loss of some superconvergence properties. However, as these configurations might appear only at a point where the curvature reaches a local extremum, they are very localized and the consequences remain local. Thus, they only affect the superconvergence properties in maximum norm. In particular, for free boundary problems, these

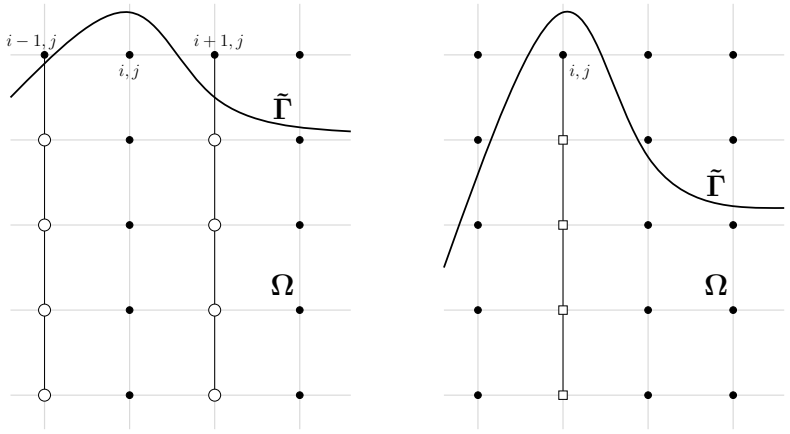

(a) alternative discretization

(b) direct extrapolation of the solution

Figure 5: Pathological configurations for the second derivative discretization

pathological local errors, which may appear in the velocity computation, do not accumulate since the interface is moving. As a result, the loss of superconvergence properties in maximum norm is localized in time and somehow compensated by the dynamics.

2.7 Issue of the interface location

It has been assumed so far that the interface location was exactly known and that θ_x and θ_y were exactly computed. Assume now that the expression that gives the zero of the level set function ψ is too complicated to get explicitely the distances $\theta_x\, h$ and $\theta_y\, h$. Or assume that ψ is an approximate of $\tilde{\psi}$, in the case of a free boundary problem for instance: the interface location is not exactly known. The distance to the interface should be computed with sufficient accuracy, so that the accuracy of the ghost values involved in the second derivative and Neumann condition computation is not disturbed. Thereby, for the L-scheme, the level set function ψ should be second order accurate at least, and θ_x and θ_y should be computed at the order 1. In the example of Figure 2, we could use

$$\theta_x = \frac{\psi_i}{\psi_i - \psi_{i-1}}. \tag{28}$$

The Q-scheme requires a third order accuracy of the level set function and a second order accuracy for θ_x and θ_y while the C-scheme requires a fourth order accuracy of the level set function and a third order accuracy for θ_x and θ_y, in order to preserve the superconvergence properties. Assume that the accuracy of the level set is sufficient. For the sake of simplicity, θ_x and θ_y are always computed at the order 3 from the values of the level set function at some grid points: this is approximated with a third order polyomial in the Lagrangian form. Denoting by $\alpha\, h$ the distance between the point x_i and any other point x_α of the same x-axis, the polynomial is given by

$$\begin{aligned} P(\alpha) =& \frac{1}{6}(\psi^h_{i-2} - 3\psi^h_{i-1} + 3\psi^h_i - \psi^h_{i+1})\alpha^3 + \frac{1}{2}(\psi^h_{i-1} - 2\psi^h_i + \psi^h_{i+1})\alpha^2 \\ &+ \frac{1}{6}(-\psi^h_{i-2} + 6\psi^h_{i-1} - 3\psi^h_i - 2\psi^h_{i+1})\alpha + \psi^h_i. \end{aligned} \tag{29}$$

Then the Newton method, initialized with (28), gives θ_x with the right accuracy. However, the assumption on the level set accuracy is very drastic for most interface problems. As for the accuracy of the data g, a refinement is addressed in Section 4.2.

3 Numerical results for 2D-problems

In this section, we present the main results of superconvergence using the schemes presented so far. The computational domain is $\tilde{\mathcal{D}} = [-0.5, 0.5] \times [-0.5, 0.5]$. All along this section, (x, y) denotes the Cartesian coordinates and (r, θ) the corresponding polar coordinates:

$$(x, y) := (r\cos(\theta), r\sin(\theta)).$$

By abuse of notation, for any domain ω of $\mathbb{R}^2$ we write

$$(r, \theta) \in \omega \quad \text{for} \quad (r\cos(\theta), r\sin(\theta)) \in \omega.$$

We first provide a result of partial superconvergence with the L-scheme. Next, we review the results of superconvergence depending on the scheme used, first with a Dirichlet condition and then with a Neumann or Robin condition. The results are obtained from exact or approximate boundary data, for various shapes of the area that are disturbed or not, and they are compared to an exact solution if it is known or a reference solution otherwise. Unless otherwise stated, for each Figure illustrating the tests of accuracy on the solution and its derivatives with convergence curves, the legend is given by

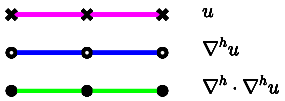

3.1 Convergence and partial superconvergence with the L-scheme

3.1.1 Test-case 1

Consider the Dirichlet problem with an exact solution given by

$$\tilde{u} = x^2 \cos\left(\pi(4\,x + y)\right), \quad \text{in } \tilde{\Omega},$$

so that $\tilde{\Omega}$ is the inner area bounded by $\tilde{\Gamma}$, the circle with center $(0, 0)$ and radius 0.25. The distances to the interface are exactly known, as well as $\tilde{f}$ and $\tilde{g}$, which are the Laplacian of $\tilde{u}$ and its Dirichlet trace on $\tilde{\Gamma}$. Table 1 shows the second order accuracy of the numerical solution on Ω. As expected, the gradient is at order 2 in L^1-norm and at order 1 in maximum norm. Still computing the solution on Ω, we restrain now the accuracy test to the disk of radius 0.21. Table 2 shows the partial superconvergence at the order 2 in maximum norm of the gradient and its divergence in the truncated area.

Number	u				$\nabla^h u$			
of points	L^1-error	order	L^∞-error	order	L^1-error	order	L^∞-error	order
64	1.112×10^{-5}	-	2.066×10^{-4}	-	8.532×10^{-4}	-	6.598×10^{-2}	-
96	4.765×10^{-6}	2.09	9.662×10^{-5}	1.87	3.966×10^{-4}	1.89	4.360×10^{-2}	1.02
144	2.140×10^{-6}	2.03	4.430×10^{-5}	1.90	1.821×10^{-4}	1.90	2.934×10^{-2}	1.00
216	9.567×10^{-7}	2.02	2.016×10^{-5}	1.91	8.345×10^{-5}	1.91	2.000×10^{-2}	0.98

Table 1: L-scheme for the Dirichlet problem on the disk of radius 0.25.

Number	$\nabla^h u$				$\nabla^h \cdot \nabla^h u$			
of points	L^1-error	order	L^∞-error	order	L^1-error	order	L^∞-error	order
64	1.925×10^{-4}	-	3.811×10^{-3}	-	1.303×10^{-2}	-	1.873×10^{-1}	-
96	8.903×10^{-5}	1.90	1.771×10^{-3}	1.89	5.930×10^{-3}	1.94	8.356×10^{-2}	1.99
144	3.939×10^{-5}	1.96	7.812×10^{-4}	1.95	2.634×10^{-3}	1.97	3.727×10^{-2}	1.99
216	1.742×10^{-5}	1.98	3.466×10^{-4}	1.97	1.169×10^{-3}	1.98	1.659×10^{-2}	1.99

Table 2: Partial superconvergence on the disk of radius 0.21.

3.2 Superconvergence for the Dirichlet problem

3.2.1 Test-case 2

Consider the same problem as for Test-case 1, using the Q-scheme and the C-scheme. Table 3 shows the results of the numerical accuracy tests on Ω: the Q-scheme generates the superconvergence of the gradient while the C-scheme gives the superconvergence of the gradient and its divergence, in maximum norm. Note that absolute errors are smaller with the C-scheme than with the Q-scheme. Figure 6 shows the convergence curves of the solution, its gradient and the divergence of its gradient in maximum norm and logarithmic scale.

Number	$\nabla^h u$				$\nabla^h \cdot \nabla^h u$			
of points	L^1-error	order	L^∞-error	order	L^1-error	order	L^∞-error	order
64	5.692×10^{-4}	-	2.149×10^{-2}	-	5.079×10^{-2}	-	2.718×10^{0}	-
96	2.312×10^{-4}	2.22	9.814×10^{-3}	1.93	2.355×10^{-2}	1.90	1.831×10^{0}	0.97
144	9.730×10^{-5}	2.18	4.421×10^{-3}	1.95	1.087×10^{-2}	1.90	1.229×10^{0}	0.98
216	4.180×10^{-5}	2.15	1.977×10^{-3}	1.96	4.931×10^{-3}	1.92	8.229×10^{-1}	0.98
64	4.211×10^{-4}	-	6.206×10^{-3}	-	2.149×10^{-2}	-	5.927×10^{-1}	-
96	1.870×10^{-4}	2.00	2.816×10^{-3}	1.95	9.135×10^{-3}	2.11	2.700×10^{-1}	1.94
144	8.406×10^{-5}	1.99	1.272×10^{-3}	1.95	3.991×10^{-3}	2.08	1.187×10^{-1}	1.98
216	3.787×10^{-5}	1.98	5.709×10^{-4}	1.96	1.759×10^{-3}	2.06	5.314×10^{-2}	1.98

Table 3: Q-scheme (top) and C-scheme (bottom) for the Dirichlet problem on the disk of radius 0.25 (Test-case 2).

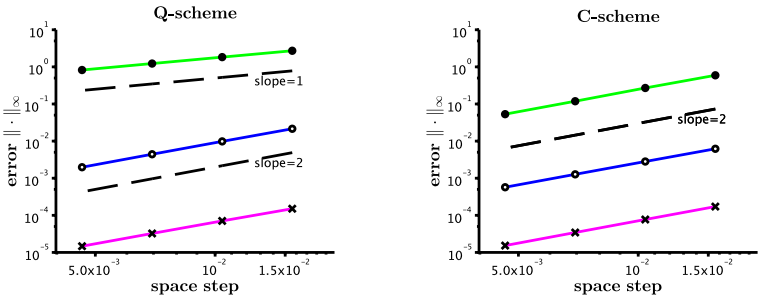

Figure 6: Convergence curves in maximum norm for Test-case 2.

3.2.2 Test-case 3

In this paragraph, the domain $\tilde{\Omega}$ is the inner area bounded by the ellipse $\tilde{\Gamma}$, with radii $r_x = 0.35$ and $r_y = 0.2$. For each point close to the interface, θ_x and θ_y are computed at the order 3. The second member of the discretized equation is given by $f = \tilde{f} = 0$. The boundary data g is extrapolated as indicated in Section 2.5, from the external field:

$$G = \ln(2 + x)\sin(2\pi y).$$

The error is computed from a reference solution on a 1000×1000 grid. Table 4 and convergence curves in Figure 7 show the results of the numerical accuracy tests for the L-scheme, the Q-scheme and the C-scheme, in maximum norm. They highlight the results of convergence and superconvergence for each numerical method.

Number of points	u L^∞-error	order	$\nabla^h u$ L^∞-error	order	$\nabla \cdot \nabla^h u$ L^∞-error	order
64	5.625×10^{-3}	-	1.449×10^{-1}	-	4.324×10^{0}	-
96	2.248×10^{-3}	2.26	8.720×10^{-2}	1.25	4.148×10^{0}	0.10
144	1.082×10^{-3}	2.03	6.196×10^{-2}	1.05	4.349×10^{0}	−0.01
216	5.070×10^{-4}	1.98	4.174×10^{-2}	1.02	4.205×10^{0}	0.07
64	1.853×10^{-4}	-	1.392×10^{-2}	-	6.253×10^{-1}	-
96	8.319×10^{-5}	1.98	6.515×10^{-3}	1.87	4.524×10^{-1}	0.80
144	2.527×10^{-5}	2.46	2.751×10^{-3}	2.00	3.254×10^{-1}	0.81
216	7.513×10^{-6}	2.64	1.263×10^{-3}	1.97	2.385×10^{-1}	0.79
64	5.562×10^{-5}	-	2.880×10^{-3}	-	2.326×10^{-1}	-
96	9.838×10^{-6}	4.27	1.033×10^{-3}	2.53	1.129×10^{-1}	1.78
144	2.084×10^{-6}	4.05	3.475×10^{-4}	2.61	3.736×10^{-2}	2.26
216	4.473×10^{-7}	3.96	1.210×10^{-4}	2.61	2.444×10^{-2}	1.85

Table 4: L-scheme (top), Q-scheme (middle) and C-scheme (bottom) for the Dirichlet problem in an ellipse (Test-case 3).

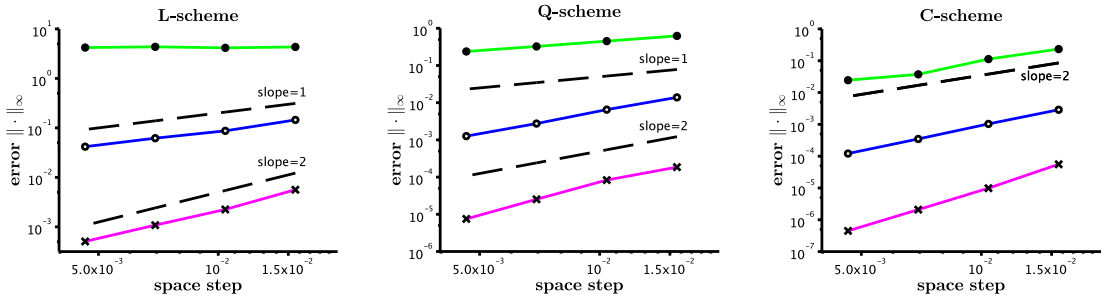

Figure 7: Convergence curves in maximum norm for Test-case 3.

Note in Table 5 and Figure 8 that computing θ_x and θ_y at the order 2 or 1 –which means disturbing $\tilde{\Gamma}$ at the order 3 or 2– leads to the loss of some superconvergence properties.

3.2.3 Test-case 4

Consider $\tilde{\Gamma}$ implicitely defined by the level 0 of the level set function $\tilde{\psi}$, in polar coordinates:

$$\tilde{\psi}(r, \theta) = r + 0.65\,\cos^2(1.25\,\theta)\,\sin^2(1.25\,\theta) - 0.4, \quad \text{in } \tilde{\mathcal{D}},$$

with the exact solution given by

$$\tilde{u} = 0.1\,\left(1 + \cos\left(3\pi(x + y)\right)\cos\left(\pi(x + 0.3)\right)\right),$$

Number of points	$\nabla^h u$ L^∞-error	order	$\nabla^h \cdot \nabla^h u$ L^∞-error	order
64	2.919×10^{-3}	-	2.435×10^{-1}	-
96	1.344×10^{-3}	1.91	1.592×10^{-1}	1.05
144	4.924×10^{-4}	2.19	8.050×10^{-2}	1.37
216	1.795×10^{-4}	2.29	5.076×10^{-2}	1.29
64	5.635×10^{-3}	-	5.717×10^{-1}	-
96	7.820×10^{-3}	-0.81	8.962×10^{-1}	-1.11
144	5.273×10^{-3}	0.08	1.758×10^{0}	-1.39
216	3.234×10^{-3}	0.46	1.358×10^{0}	-0.71

Table 5: Loss of superconvergence properties of the C-scheme, for Test-case 3, if θ is at the order 2 (top) or at the order 1 (bottom).

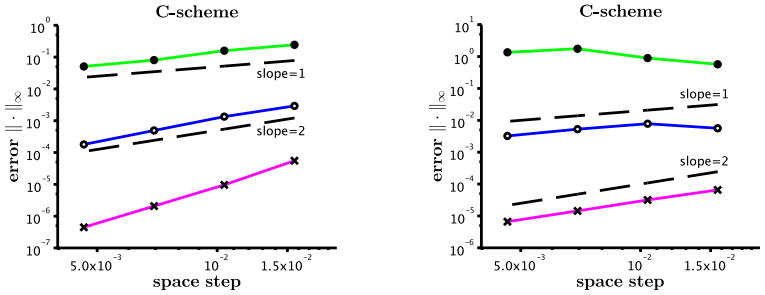

Figure 8: C-scheme, for Test-case 3, with θ at the order 2 (left) and at the order 1 (right).

in the inner area $\tilde{\Omega}$. $\tilde{f}$ and $\tilde{g}$ are explicitly inferred from $\tilde{u}$ as its Laplacian and its trace on $\tilde{\Gamma}$. A plot of the numerical solution u, computed with the L-scheme on a 324×324 grid, is provided in Figure 9. Table 6 and convergence curves in Figure 10 show the results of the numerical accuracy tests for the L-scheme, the Q-scheme and the C-scheme, in maximum norm.

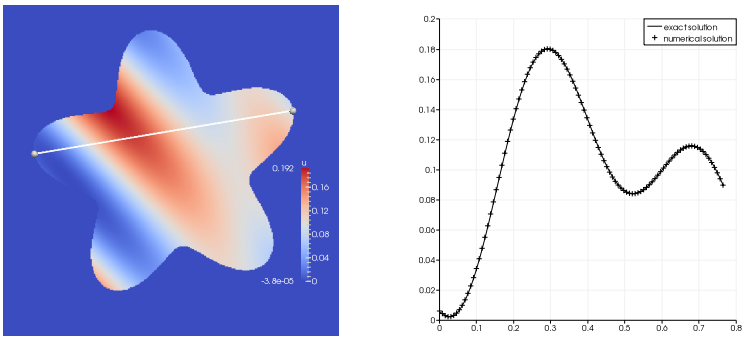

Figure 9: Numerical solution of Test-case 4 with L-scheme. Left: solution computed on a 324×324 grid. Right: solution along the section line. The solid line is the exact solution, the plus are the numerical solution.

Note that the values of θ_x and θ_y are computed at the order 3 in this example. However, taking the trace of the exact solution as the boundary data overcomes the need to have a good precision on the interface location. Whatever the accuracy of θ_x and θ_y, the numerical scheme behaves as if they were known exactly, in contrast to the test-case 3 computed from a reference solution.

Number of points	u L^∞-error	order	$\nabla^h u$ L^∞-error	order	$\nabla \cdot \nabla^h u$ L^∞-error	order
96	1.198×10^{-4}	-	6.862×10^{-2}	-	9.555×10^{0}	-
144	5.304×10^{-5}	2.01	4.650×10^{-2}	0.96	9.479×10^{0}	0.02
216	2.395×10^{-5}	1.99	3.117×10^{-2}	0.97	9.450×10^{0}	0.01
324	9.752×10^{-6}	2.06	2.085×10^{-2}	0.98	9.415×10^{0}	0.01
96	8.377×10^{-5}	-	5.254×10^{-3}	-	1.479×10^{0}	-
144	3.713×10^{-5}	2.01	2.379×10^{-3}	1.95	9.803×10^{-1}	1.01
216	1.646×10^{-5}	2.01	1.057×10^{-3}	1.98	6.495×10^{-1}	1.01
324	7.301×10^{-6}	2.01	4.661×10^{-4}	1.99	4.369×10^{-1}	1.00
96	8.290×10^{-5}	-	2.843×10^{-3}	-	1.819×10^{-1}	-
144	3.684×10^{-5}	2.00	1.177×10^{-3}	2.17	7.931×10^{-2}	2.05
216	1.637×10^{-5}	2.00	4.927×10^{-4}	2.16	3.415×10^{-2}	2.06
324	7.273×10^{-6}	2.00	2.167×10^{-4}	2.12	1.519×10^{-2}	2.04

Table 6: L-scheme (top), Q-scheme (middle) and C-scheme (bottom) for the Dirichlet problem of Test-case 4.

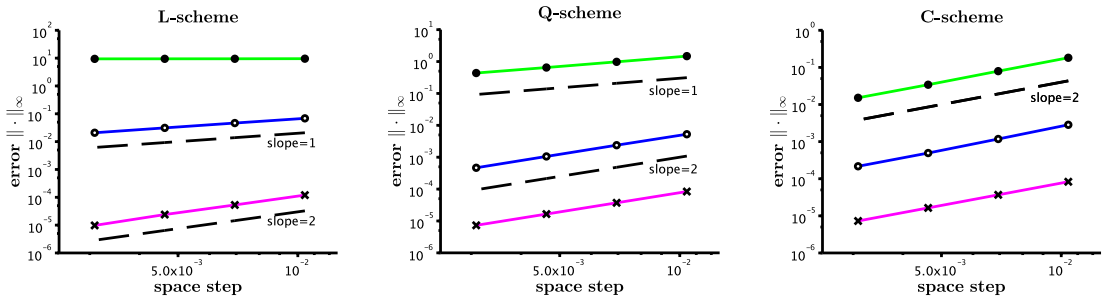

Figure 10: Convergence curves in maximum norm for Test-case 4.

3.2.4 Test-case 5

Consider the same simple problem as for Test-cases 1 and 2, and let perturb the exact data $\tilde{f}$, $\tilde{g}$ and $\tilde{\psi}$ as mentionned in Section 2. The perturbations are built by adding oscillating functions. They are defined by

$$f = \tilde{f} + 10 \sin\left(\frac{x}{h}\right) h^2, \quad \text{in } \Omega, \tag{30}$$

$$g = \tilde{g} + \cos\left(\frac{x}{h}\right) \sin\left(\frac{y}{h}\right) h^p, \quad \text{on } \Gamma, \tag{31}$$

$$\psi = \tilde{\psi} + \left[\sin\left(\frac{x+0.5}{h}\right) + \cos\left(\frac{y+0.5}{h}\right)\right] h^q, \quad \text{in } \mathcal{D}. \tag{32}$$

The second-member of the equation $\tilde{f}$ is perturbed at the order 2 in order to preserve the operator consistency at each grid point. The boundary data $\tilde{g}$ and the level set function $\tilde{\psi}$ are perturbed at the order $p = q = 2$ for the L-scheme, $p = q = 3$ for the Q-scheme and $p = q = 4$ for the C-scheme. Table 7 shows the results of the numerical accuracy tests for the three schemes, in maximum norm. As expected, the perturbations do not significantly affect the superconvergence properties.

3.3 Superconvergence for the Neumann and Robin problems

3.3.1 Test-case 6

Consider $\tilde{\Gamma}$, the circle with center $(0, 0)$ and radius 0.25 and $\tilde{\Omega}$, the outer area. The Poisson equation is given on $\tilde{\Omega}$ with a Robin condition on $\tilde{\Gamma}$ defined by the function $\rho(x, y) = 4\,x\,y$ and

Number of points	u L^∞-error	order	$\nabla^h u$ L^∞-error	order	$\nabla \cdot \nabla^h u$ L^∞-error	order
64	3.494×10^{-4}	-	7.061×10^{-2}	-	6.167×10^{0}	-
96	1.238×10^{-4}	2.56	4.468×10^{-2}	1.13	5.552×10^{0}	0.26
144	5.582×10^{-5}	2.26	3.018×10^{-2}	1.05	5.191×10^{0}	0.21
216	3.141×10^{-5}	1.98	2.129×10^{-2}	0.99	5.275×10^{0}	0.13
64	1.508×10^{-4}	-	2.156×10^{-2}	-	2.719×10^{0}	-
96	7.076×10^{-5}	1.87	9.831×10^{-3}	1.94	1.832×10^{0}	0.97
144	3.244×10^{-5}	1.89	4.428×10^{-3}	1.95	1.230×10^{0}	0.98
216	1.472×10^{-5}	1.91	1.982×10^{-3}	1.96	8.238×10^{-1}	0.98
64	1.726×10^{-4}	-	6.216×10^{-3}	-	5.941×10^{-1}	-
96	7.717×10^{-5}	1.98	2.824×10^{-3}	1.95	2.706×10^{-1}	1.94
144	3.441×10^{-5}	1.99	1.274×10^{-3}	1.95	1.188×10^{-1}	1.99
216	1.530×10^{-5}	1.99	5.714×10^{-4}	1.96	5.343×10^{-2}	1.98

Table 7: L-scheme (top), Q-scheme (middle) and C-scheme (bottom) for the Dirichlet problem with perturbations on data (Test-case 5).

a Dirichlet condition on $\partial\tilde{\mathcal{D}}$. The exact solution is given in $\tilde{\Omega}$, in polar coordinates, by

$$\tilde{u}(r,\theta) = r^2\,(1+\cos\theta).$$

The second member $\tilde{f}$ of the equation, the boundary data $\tilde{g}$ on $\tilde{\Gamma}$ and the data on $\partial\tilde{\mathcal{D}}$ are explicitely inferred from $\tilde{u}$ and ρ. The numerical data ψ, f and g are the exact restrictions of $\tilde{\psi}$, $\tilde{f}$ and $\tilde{g}$ to $\mathcal{D}$, Ω and Γ, respectively. Table 8 and convergence curves in Figure 11 show the results of the numerical accuracy tests for the L-scheme, the Q-scheme and the C-scheme, in maximum norm. It is worth noting that the L-scheme for the Robin problem is a first order method and that the gradient superconverges at the order 1. The other schemes behave as for the Dirichlet problem.

Number of points	u L^∞-error	order	$\nabla^h u$ L^∞-error	order	$\nabla \cdot \nabla^h u$ L^∞-error	order
96	3.257×10^{-3}	-	2.108×10^{-2}	-	3.583×10^{0}	-
144	2.226×10^{-3}	0.94	1.363×10^{-2}	1.08	3.518×10^{0}	0.05
216	1.342×10^{-3}	1.09	1.076×10^{-2}	0.83	3.516×10^{0}	0.02
324	8.936×10^{-4}	1.06	6.920×10^{-3}	0.92	3.586×10^{0}	-0.00
96	1.069×10^{-5}	-	5.441×10^{-4}	-	9.205×10^{-2}	-
144	5.425×10^{-6}	1.67	2.639×10^{-4}	1.78	6.285×10^{-2}	0.94
216	1.855×10^{-6}	2.16	1.113×10^{-4}	1.96	4.211×10^{-2}	0.96
324	8.208×10^{-7}	2.11	5.404×10^{-5}	1.90	2.975×10^{-2}	0.93
96	4.634×10^{-6}	-	1.696×10^{-4}	-	5.256×10^{-3}	-
144	2.041×10^{-6}	2.02	7.581×10^{-5}	1.99	1.564×10^{-3}	2.99
216	8.904×10^{-7}	2.03	3.400×10^{-5}	1.98	1.062×10^{-3}	1.97
324	3.943×10^{-7}	2.03	1.513×10^{-5}	1.99	4.407×10^{-4}	2.04

Table 8: L-scheme (top), Q-scheme (middle) and C-scheme (bottom) for the Robin problem on the disk of radius 0.25 (Test-case 6).

3.3.2 Test-case 7

Consider the same problem as for Test-case 6, with perturbations defined by (30), (31) and (32). Once again, the superconvergence properties are not affected by the perturbations. The results of the numerical accuracy tests are very similar to those of Test-case 6. We just provide the convergence curves in Figure 12.

3.3.3 Test-case 8

Consider now $\tilde{\Gamma}$ implicitely defined as the level 0 of $\tilde{\psi}$ in polar coordinates:

$$\tilde{\psi}(r,\theta) = -r - 0.3\,\cos^2(\theta+\frac{\pi}{4}) + 0.4,$$

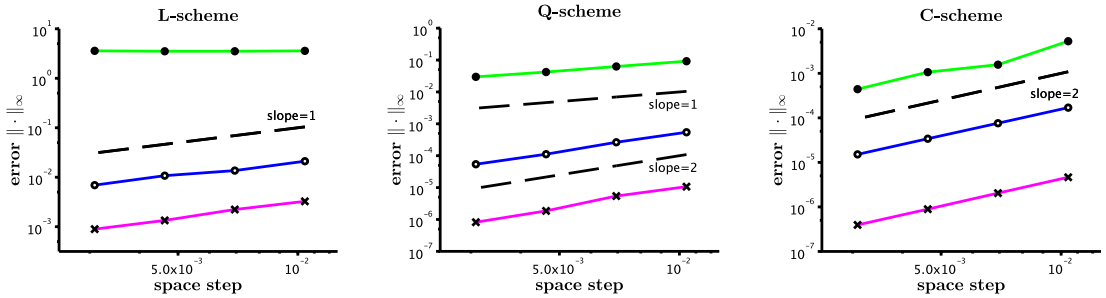

Figure 11: Convergence curves in maximum norm for Test-case 6.

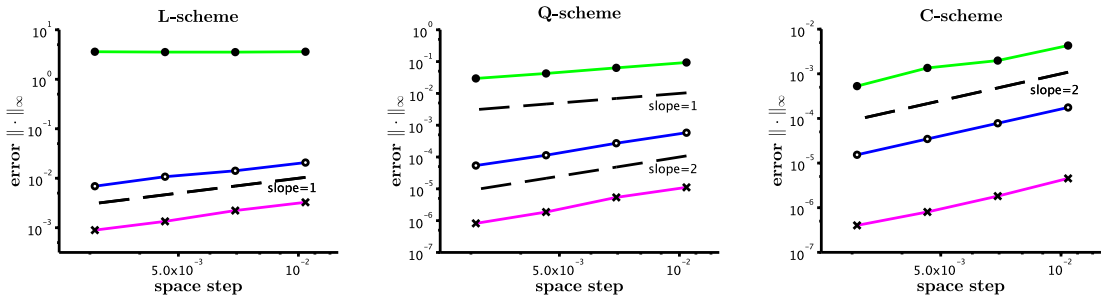

Figure 12: Convergence curves in maximum norm for the Robin problem with perturbed data (Test-case 7).

with the exact solution of the Neumann problem ($\rho = 0$), given by

$$\tilde{u} = x^2 \sin(2\,\pi\, y)\,,$$

in the outer area $\tilde{\Omega}$, where $\tilde{\psi} < 0$. $\tilde{f}$ and the Dirichlet data on $\partial\tilde{\mathcal{D}}$ are explicitly inferred from $\tilde{u}$. $\tilde{g}$ is explicitely inferred from $\tilde{u}$ and from the normal vector that is exactly computed from $\tilde{\psi}$, rewritten in Cartesian coordinate. f and g, the restrictions of $\tilde{f}$ and $\tilde{g}$ to Ω and Γ, are exact. A plot of the numerical solution u, computed with the Q-scheme on a 324×324 grid, is provided in Figure 13. Table 9 and convergence curves in Figure 14 show the results of the numerical

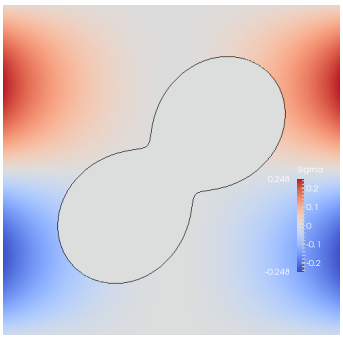

Figure 13: Numerical solution of Test-case 8 with the Q-scheme.

accuracy tests for the L-scheme, the Q-scheme and the C-scheme, in maximum norm.

Number of points	u L^∞-error	order	$\nabla^h u$ L^∞-error	order	$\nabla \cdot \nabla^h u$ L^∞-error	order
96	9.037×10^{-4}	-	3.249×10^{-2}	-	1.403×10^{0}	-
144	6.068×10^{-4}	0.98	2.039×10^{-2}	1.15	1.413×10^{0}	-0.02
216	3.955×10^{-4}	1.02	1.450×10^{-2}	0.99	1.511×10^{0}	-0.09
324	2.638×10^{-4}	1.01	9.594×10^{-3}	1.00	1.495×10^{0}	-0.05
96	4.251×10^{-5}	-	2.204×10^{-3}	-	4.742×10^{-1}	-
144	1.744×10^{-5}	2.20	9.856×10^{-4}	1.98	3.184×10^{-1}	0.98
216	7.589×10^{-6}	2.12	4.398×10^{-4}	1.99	2.133×10^{-1}	0.99
324	3.607×10^{-6}	2.03	1.960×10^{-4}	1.99	1.427×10^{-1}	0.99
96	4.415×10^{-5}	-	1.093×10^{-3}	-	2.172×10^{-2}	-
144	1.994×10^{-5}	1.96	4.908×10^{-4}	1.97	1.188×10^{-2}	1.49
216	8.858×10^{-6}	1.98	2.196×10^{-4}	1.98	3.856×10^{-3}	2.13
324	3.991×10^{-6}	1.98	9.807×10^{-5}	1.98	1.358×10^{-3}	2.28

Table 9: L-scheme (top), Q-scheme (middle) and C-scheme (bottom) for the Neumann problem of Test-case 8.

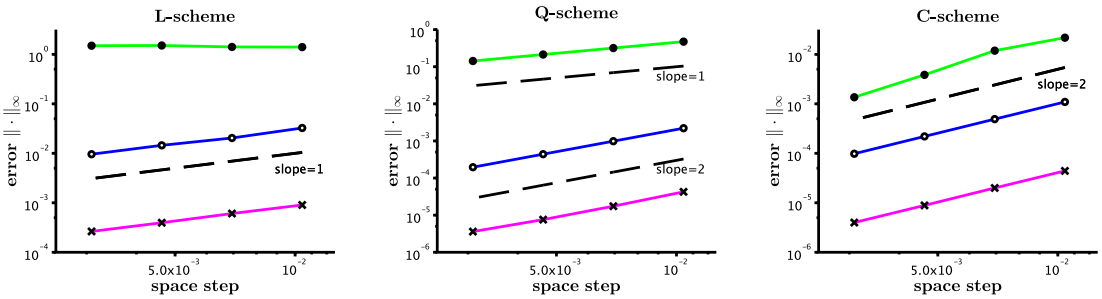

Figure 14: Convergence curves in maximum norm for Test-case 8.

4 Numerical results for coupled problems

We have numerically highlighted the superconvergence properties with an accuracy on the data g and ψ at the order 3 for the Q-scheme and order 4 for the C-scheme. However, if problems are coupled and solved with any second order (or first order) methods, we can not expect better than a second order (or first order) accuracy on the data, especially g and ψ. For instance, the second order solution of one problem may give the boundary data of the second problem, that can not be more accurate than order 2. In this section, refinements are proposed throughout numerical tests –but without the proof being established– for Dirichlet and Neumann or Robin problems, in order to preserve the superconvergence even with less accurate data, that have themselves some superconvergent properties. Some numerical accuracy tests for coupled problems are also provided: a Neumann problem coupled with a Dirichlet problem and at last, a dynamical coupled problem applied to biology.

4.1 Transmission of superconvergence properties

4.1.1 Test-case 9

Consider the perturbated Dirichlet problem of Test-case 5. Keep the perturbations defined by (30)-(32). Keep $q = 3$ and 4 in (32) for the Q-scheme and the C-scheme, respectively, but set $p = 2$ in (31), instead of $p = 3$ and $p = 4$. The location of the interface remains third or fourth order accurate while the boundary data g is at the order 2. Figure 15 shows the results of the numerical accuracy tests. As expected, the superconvergence properties are perturbated for the Q-scheme and the C-scheme if g is at the order 2. Note that for the C-scheme with a third order

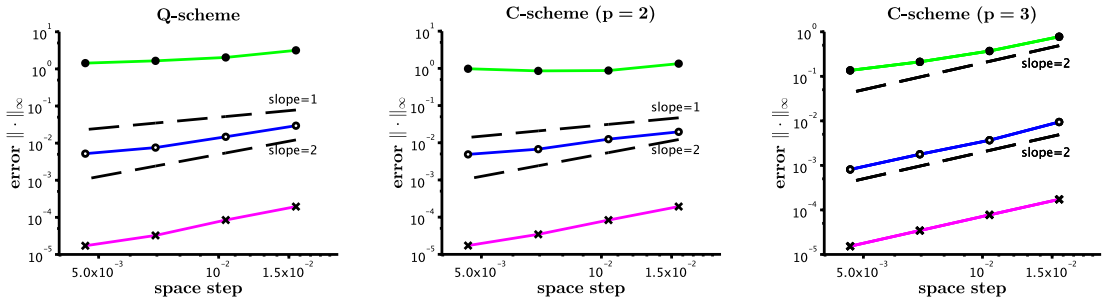

Figure 15: Loss of superconvergence properties for Q-scheme (left) and C-scheme (middle) if g is only second order accurate ($p = 2$). On the right, the same problem is solved with the C-scheme and $p = 3$: g is at the order 3 (Test-case 9).

perturbation on $\tilde{g}$ (p=3), only the superconvergence of the second derivative is slightly affected. Replace now the oscillating perturbation (31) on $\tilde{g}$ by a more regular (non-oscillating) one, at the order 2 for both Q and C-schemes:

$$g = \tilde{g} + \cos(x)\,\sin(y)\,h^2, \quad \text{on } \Gamma. \tag{33}$$

It is a way to build superconvergent approximate data from the exact data. This means that g remains at the order 2 and each of its numerical tangential derivatives (defined in the same spirit as for the normal derivative, at the order 2) are also second order accurate with respect to the tangential derivatives of $\tilde{g}$. Table 10 shows the results of the numerical accuracy tests. Surprisingly, the superconvergence properties are well preserved.

Number of points	u L^∞-error	order	$\nabla^h u$ L^∞-error	order	$\nabla \cdot \nabla^h u$ L^∞-error	order
64	1.594×10^{-4}	-	2.153×10^{-2}	-	2.721×10^{0}	-
96	7.407×10^{-5}	1.89	9.817×10^{-3}	1.94	1.832×10^{0}	0.97
144	3.384×10^{-5}	1.91	4.424×10^{-3}	1.95	1.229×10^{0}	0.98
216	1.533×10^{-5}	1.92	1.978×10^{-3}	1.96	8.231×10^{-1}	0.98
64	1.794×10^{-4}	-	6.270×10^{-3}	-	5.942×10^{-1}	-
96	8.015×10^{-5}	1.99	2.822×10^{-3}	1.97	2.707×10^{-1}	1.94
144	3.573×10^{-5}	1.99	1.274×10^{-3}	1.97	1.187×10^{-1}	1.99
216	1.589×10^{-5}	1.99	5.720×10^{-4}	1.97	5.342×10^{-2}	1.98

Table 10: Q-scheme (top) and C-scheme (bottom) with a second order non-oscillating perturbation on $\tilde{g}$ for the Dirichlet problem of Test-case 9.

We also obtain the same results by refining the perturbation:

$$g = \tilde{g} + \cos(x)\,\sin(y)\,h^2 + \cos\left(\frac{x}{h}\right)\,\sin\left(\frac{y}{h}\right)\,h^p, \quad \text{on } \Gamma, \tag{34}$$

with $p = 3$ for the Q-scheme and $p = 4$ for the C-scheme. For the Q-scheme, this means that g and its first numerical tangential derivative are second order accurate, but not its higher-order derivatives. For the C-scheme, only g and its first and second tangential derivatives are at the order 2. Note that if g is computed as described in Section 2.5, from an external field G, a second order accuracy on G and its derivatives also generates the same results. Computing g with a third order extrapolation, for the Q-scheme, preserves the second order accuracy on g and $\partial^h_\tau g$, while the fourth order extrapolation, for the C-scheme, preserves the second order accuracy on g, $\partial^h_\tau g$ and $\partial^h_{\tau\tau} g$. Those results give criteria of accuracy, depending on the scheme used, that are required for g and its tangential derivatives (or G and its derivatives) to ensure superconvergence for a Poisson problem with a Dirichlet condition. They are summarized in Table 11.

	data accuracy			solution accuracy		
	g	$\partial_\tau^h g$	$\partial_{\tau\tau}^h g$	u	$\nabla^h u$	$\nabla^h \cdot \nabla^h u$
L-scheme	2			2	1	0
Q-scheme	2	2		2	2	1
C-scheme	2	2	2	2	2	2

Table 11: Order of accuracy of the boundary data (left) required to obtain superconvergence properties (right) for a Dirichlet problem, with respect to the considered numerical scheme.

4.1.2 Test-case 10

Consider the same perturbated Robin problem as for Test-case 7, just modifying the perturbation on $\tilde{g}$. In Test-case 7, the exact boundary data $\tilde{g}$ is perturbed with the same principle as for Dirichlet problems, described in Section 2.5. However, the term $2\,h\,g$ in relation (27) suggests that g can be one order of accuracy lower than the data of Dirichlet problems, without affecting the required accuracy of the numerical solution interface value. The perturbation given by (31) is therefore tested with $p = 1$ for the L-scheme, $p = 2$ for the Q-scheme and $p = 3$ for the C-scheme. As a result of the numerical accuracy tests, Table 12 shows that the less drastic accuracy of g does not impact the superconvergence of the solution. Note that the first order

Number of points	u L^∞-error	order	$\nabla^h u$ L^∞-error	order	$\nabla \cdot \nabla^h u$ L^∞-error	order
96	3.443×10^{-3}	-	2.443×10^{-2}	-	3.756×10^{0}	-
144	2.244×10^{-3}	1.06	1.665×10^{-2}	0.95	3.820×10^{0}	−0.04
216	1.373×10^{-3}	1.13	1.206×10^{-2}	0.87	3.693×10^{0}	0.02
324	9.003×10^{-4}	1.10	8.478×10^{-3}	0.87	3.756×10^{0}	−0.00
96	1.372×10^{-5}	-	6.038×10^{-4}	-	9.556×10^{-2}	-
144	5.962×10^{-6}	2.05	2.980×10^{-4}	1.74	6.639×10^{-2}	0.90
216	1.939×10^{-6}	2.41	1.311×10^{-4}	1.88	4.500×10^{-2}	0.93
324	9.152×10^{-7}	2.23	6.023×10^{-5}	1.89	3.094×10^{-2}	0.93
96	4.532×10^{-6}	-	1.762×10^{-4}	-	4.330×10^{-3}	-
144	1.819×10^{-6}	2.25	7.803×10^{-5}	2.01	2.013×10^{-3}	1.89
216	8.028×10^{-7}	2.13	3.470×10^{-5}	2.00	1.359×10^{-3}	1.43
324	4.018×10^{-7}	1.99	1.534×10^{-5}	2.01	5.360×10^{-4}	1.72

Table 12: L-scheme ($p = 1$, top), Q-scheme ($p = 2$, middle) and C-scheme ($p = 3$, bottom) for the perturbated Neumann problem of Test-case 10.

and the second order of accuracy on g are sufficient to ensure the expected properties of the L-scheme and the Q-scheme, respectively. If (31) is replaced by (34), with $p = 4$, g, $\partial_\tau g$ and $\partial_{\tau\tau} g$ are second order accurate. If $p = 3$, only g and $\partial_\tau g$ are second order accurate. Both cases are tested for the C-scheme and give very similar results. Table 13 shows the results for the case $p = 3$ of the numerical accuracy tests. Once again, the superconvergence of the gradient of the numerical solution and its divergence is ensured. Figure 16 shows the convergence curves

Number of points	u L^∞-error	order	$\nabla^h u$ L^∞-error	order	$\nabla \cdot \nabla^h u$ L^∞-error	order
96	7.550×10^{-6}	-	1.822×10^{-4}	-	4.326×10^{-3}	-
144	3.299×10^{-6}	2.04	8.051×10^{-5}	2.01	2.013×10^{-3}	1.89
216	1.452×10^{-6}	2.03	3.585×10^{-5}	2.00	1.359×10^{-3}	1.43
324	6.555×10^{-7}	2.01	1.575×10^{-5}	2.01	5.360×10^{-4}	1.72

Table 13: Numerical results with the C-scheme for the Neumann problems of Test-case 10 with perturbation (34) and $p = 3$.

for the three different schemes with the boundary data of minimal accuracy: g is at the order 1

for the L-scheme and order 2 for the Q-scheme. For the C-scheme, g is perturbed with (34) and $p = 3$. As for the Dirichlet problem, we summarize in Table 14 the criteria of accuracy required

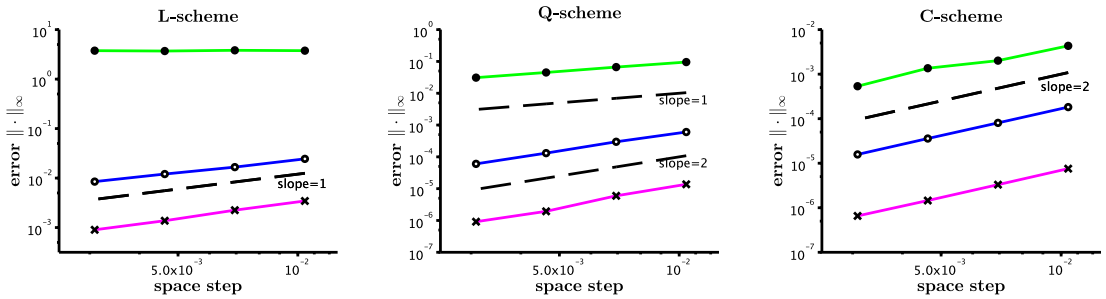

Figure 16: L-scheme, Q-scheme and C-scheme with the boundary data of minimal accuracy (Test-case 10).

for g and its tangential derivatives to ensure superconvergence for the Poisson problem with a Neumann or Robin condition.

	data accuracy			solution accuracy		
	g	$\partial^h_\tau g$	$\partial^h_{\tau\tau} g$	u	$\nabla^h u$	$\nabla^h \cdot \nabla^h u$
L-scheme	1			1	1	0
Q-scheme	2			2	2	1
C-scheme	2	2		2	2	2

Table 14: Order of accuracy of the boundary data (left) required to obtain superconvergence properties (right) for a Neumann problem, with respect to the considered numerical scheme.

4.1.3 Test-case 11

Let $\tilde{\Gamma}$ be the level 0 of the exact level set function, in polar coordinate

$$\tilde{\psi}(r,\theta) = r + 0.5\,\cos^2(\theta + \frac{\pi}{8})\,\sin^2(\theta + \frac{\pi}{8}) - 0.4.$$

$\tilde{\Gamma}$ splits the computational domain $\tilde{\mathcal{D}}$ into two areas: $\tilde{\Omega}_1$ is the outer area and $\tilde{\Omega}_2$ is the inner area. $\tilde{\mathbf{n}}$ is given by (26). Consider the continuous problem

$$\Delta \tilde{u}_1 = \tilde{f}_1, \quad \text{in } \tilde{\Omega}_1, \tag{35}$$

$$-\partial_{\mathbf{n}} \tilde{u}_1 = \tilde{g}, \quad \text{on } \tilde{\Gamma}, \tag{36}$$

$$\tilde{u}_1 = 0, \quad \text{on } \partial\tilde{\mathcal{D}}, \tag{37}$$

$$\Delta \tilde{u}_2 = \tilde{f}_2, \quad \text{in } \tilde{\Omega}_2, \tag{38}$$

$$\tilde{u}_2 = \tilde{u}_1, \quad \text{on } \tilde{\Gamma}, \tag{39}$$

For the numerical resolution, set $f_1 = \tilde{f}_1 = 0$, $f_2 = \tilde{f}_2 = 0$ and $\psi = \tilde{\psi}$ (no perturbations). The exact boundary data is given by

$$\tilde{g} = \sin^2\left(\pi\,(x+y)\right), \quad \text{on } \tilde{\Gamma} \tag{40}$$

and is assumed to be perturbed such that:

$$g = \tilde{g} + \cos\left(\frac{\pi}{2}\, x\, y\right)\, h^2 + 2\, y\, \sin\left(\frac{x}{h}\right)\, h^p, \quad \text{on } \Gamma. \tag{41}$$

The coupled problem is first solved with the L-schemes and $p = 1$, and then with the Q-schemes and $p = 2$, so that g is first order and second order accurate, respectively. Finally, it is solved with the C-schemes and $p = 3$, so that g and $\partial_\tau g$ are second order accurate. Figure 17 shows a plot of the numerical solutions computed with the C-scheme on a 486×486 grid.

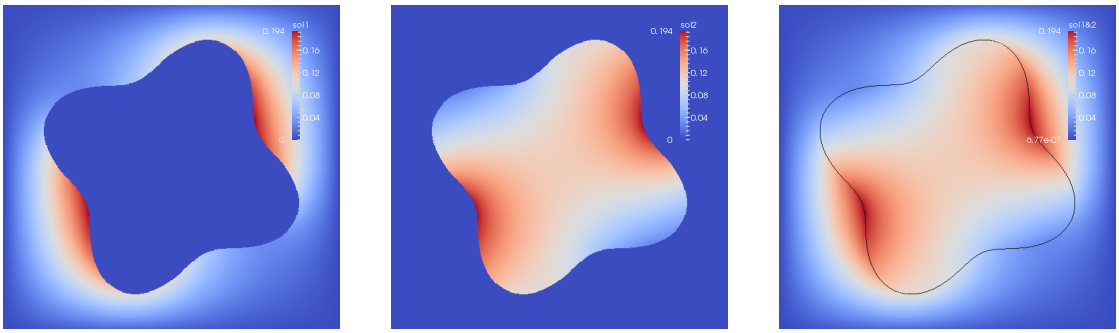

Figure 17: Numerical solution of the coupled problem of Test-case 11, computed with the C-scheme. Left: solution u_1 of the Neumann problem. Middle: solution u_2 of the Dirichlet problem. Right: merged solutions.

The errors are computed by comparing the numerical solution to a reference solution on a 1000×1000 grid, using the exact boundary data $\tilde{g}$. Table 15 and Figure 18 show the results of the numerical accuracy tests.

	Number of points	u L^∞-error	order	$\nabla^h u$ L^∞-error	order	$\nabla \cdot \nabla^h u$ L^∞-error	order
u_1	144	1.248×10^{-3}	-	3.046×10^{-2}	-	2.777×10^{0}	-
	216	8.752×10^{-4}	0.87	2.049×10^{-2}	0.98	2.754×10^{0}	0.02
	324	4.4288×10^{-4}	1.28	1.375×10^{-2}	0.98	2.948×10^{0}	−0.07
	486	1.798×10^{-4}	1.59	1.005×10^{-2}	0.91	2.827×10^{0}	−0.01
u_2	144	1.113×10^{-3}	-	5.968×10^{-2}	-	6.024×10^{0}	-
	216	8.353×10^{-4}	0.71	4.338×10^{-2}	0.79	6.121×10^{0}	−0.04
	324	4.166×10^{-4}	1.21	2.393×10^{-2}	1.13	6.291×10^{0}	−0.05
	486	1.695×10^{-4}	1.55	1.645×10^{-2}	1.06	7.988×10^{0}	−0.23
u_1	144	7.211×10^{-5}	-	3.645×10^{-3}	-	7.848×10^{-1}	-
	216	3.329×10^{-5}	1.91	1.626×10^{-3}	1.99	5.686×10^{-1}	0.79
	324	1.438×10^{-5}	1.99	7.868×10^{-4}	1.89	3.669×10^{-1}	0.94
	486	5.847×10^{-6}	2.07	3.321×10^{-4}	1.97	2.259×10^{-1}	1.02
u_2	144	6.062×10^{-5}	-	8.341×10^{-3}	-	2.684×10^{0}	-
	216	3.142×10^{-5}	1.62	4.093×10^{-3}	1.76	1.969×10^{0}	0.76
	324	1.382×10^{-5}	1.82	1.941×10^{-3}	1.80	1.121×10^{0}	1.08
	486	5.641×10^{-6}	1.95	8.831×10^{-4}	1.85	6.932×10^{-1}	1.11
u_1	144	2.955×10^{-5}	-	1.164×10^{-3}	-	2.715×10^{-1}	-
	216	1.155×10^{-5}	2.32	4.743×10^{-4}	2.21	1.472×10^{-1}	1.51
	324	4.999×10^{-6}	2.19	2.451×10^{-4}	1.92	6.857×10^{-2}	1.70
	486	1.797×10^{-6}	2.30	9.836×10^{-5}	2.03	3.055×10^{-2}	1.80
u_2	144	2.911×10^{-5}	-	3.165×10^{-3}	-	1.305×10^{0}	-
	216	1.134×10^{-5}	2.33	1.632×10^{-3}	1.63	7.635×10^{-1}	1.32
	324	4.957×10^{-6}	2.18	7.258×10^{-4}	1.82	3.514×10^{-1}	1.62
	486	1.788×10^{-6}	2.29	3.070×10^{-4}	1.92	1.516×10^{-1}	1.77

Table 15: Numerical solutions u_1 and u_2 computed with L-schemes (top), Q-schemes (middle) and C-schemes (bottom) for the coupled problem of Test-case 11.

It is worth noting that thanks to the transmission properties summarized in Tables 11 and 14,

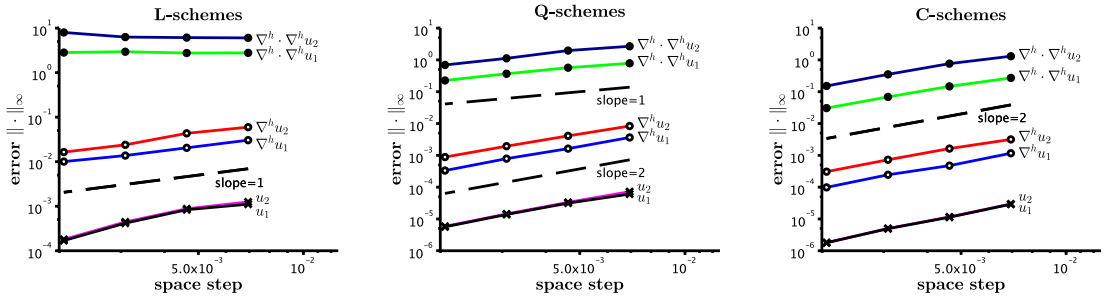

Figure 18: Accuracy results of L-scheme (left), Q-scheme (middle) and C-scheme (right) for the coupled problem of Test-case 11.

other combinations can be considered to achieve the superconvergence. Assume for instance that g is the boundary data for the Dirichlet problem whose solution gives the boundary data for the Neumann problem. Solving the Dirichlet subproblem with the Q-scheme leads to a second order accuracy for its solution and its gradient and a first order accuracy for the divergence of the gradient. Then solving the Neumann problem with the C-scheme, gives a second order accurate solution and the superconvergence at the order 2 of the gradient and its divergence.

4.2 Accuracy on the interface location

Disrupt the interface location is not equivalent to perturb the boundary data, since it also impacts the computation of the distances θ_x and θ_y. As the interface accuracy is a cornerstone for coupled problems with moving boundary, the issue has to be specifically studied.

4.2.1 Test-case 12

Consider the continuous Dirichlet problem in $\tilde{\Omega}$, the disk with center $(0,0)$ and radius 0.25. The data are given by

$$\tilde{g} = \sin^2\left(\pi\left(x+y\right)\right), \quad \text{on } \tilde{\Gamma}, \tag{42}$$

$$\tilde{f} = 0, \quad \text{in } \tilde{\Omega}. \tag{43}$$

For the numerical problem, the boundary condition g and the second member f of the equation are exactly equal to $\tilde{g}$ and $\tilde{f}$ at the grid points. The interface location is perturbed at the order 2 thanks to

$$\psi = \tilde{\psi} + \cos\left(\pi\, x\, y\right)\, h^2 + \sin\left(\frac{3\,x}{h}\right)\cos\left(\frac{2\,y}{h}\right) h^q, \quad \text{in } \mathcal{D} \tag{44}$$

so that $\nabla^h\psi$ –and therefore the numerical normal vector $\mathbf{n}$– is accurate at the order $\min(2, q-1)$, and $\nabla^h\cdot\nabla^h\psi$ is at the order $\min(2, q-2)$. θ_x and θ_y are computed at the order 3, which does not affect the perturbation (44) for $q \leq 4$. By analogy with the perturbation on the boundary condition –see previous Subsection– we set $q = 3$ for the Q-scheme and $q = 4$ for the C-scheme. Note that the case $q = 2$ for the L-scheme has already been tested in previous test-cases. The numerical solutions are compared to reference solutions that are computed on a 1000×1000 grid using the exact level set function $\tilde{\psi}$. Table 16 and Figure 19 show the results of the numerical accuracy tests. Again, the solutions keep the right superconvergence properties. Logically, using $q = 2$ for the Q-scheme and $q = 3$ for the C-scheme leads to the loss of the superconvergence

Number of points	u L^∞-error	order	$\nabla^h u$ L^∞-error	order	$\nabla \cdot \nabla^h u$ L^∞-error	order
96	4.242×10^{-4}	-	5.405×10^{-3}	-	9.954×10^{-1}	-
144	1.906×10^{-4}	1.97	2.527×10^{-3}	1.87	6.739×10^{-1}	0.96
216	8.600×10^{-5}	1.97	1.134×10^{-3}	1.93	4.483×10^{-1}	0.98
324	3.815×10^{-5}	1.98	5.129×10^{-4}	1.94	2.895×10^{-1}	1.02
96	4.206×10^{-4}	-	1.749×10^{-3}	-	8.218×10^{-2}	-
144	1.893×10^{-4}	1.97	7.736×10^{-4}	2.01	3.727×10^{-2}	1.95
216	8.557×10^{-5}	1.96	3.441×10^{-4}	2.01	1.678×10^{-2}	1.96
324	3.804×10^{-5}	1.98	1.512×10^{-4}	2.01	7.542×10^{-3}	1.96

Table 16: Q-scheme (top, $q = 3$) and C-scheme (bottom, $q = 4$) with a second order perturbation on $\tilde{\psi}$ for the Dirichlet problem of Test-case 12.

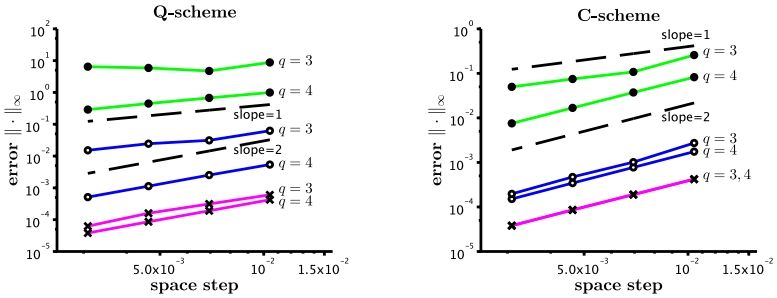

Figure 19: Numerical results for the Q-scheme with $q = 3$ and $q = 2$ (left) and for the C-scheme with $q = 4$ and $q = 3$ (right) for the Dirichlet problem of Test-case 12.

properties, as shown in Figure 19. Hence, the criteria on the interface location accuracy, required to achieve the superconvergence for a Poisson problem with a Dirichlet condition, are the same as for the boundary data accuracy. They are summarized in Table 17.

	level set accuracy			solution accuracy		
	ψ	$\nabla^h \psi$	$\nabla^h \cdot \nabla^h \psi$	u	$\nabla^h u$	$\nabla^h \cdot \nabla^h u$
L-scheme	2			2	1	0
Q-scheme	2	2		2	2	1
C-scheme	2	2	2	2	2	2

Table 17: Order of accuracy of the interface location (left) required to obtain superconvergence properties (right) for a Dirichlet problem, with respect to the considered numerical scheme.

4.2.2 Test-case 13

Consider the Neumann problem in $\tilde{\Omega}$, the outer area, where $\tilde{\psi}$ is negative:

$$\tilde{\psi}(r, \theta) = -r - 0.3 \cos^2(\theta + \frac{\pi}{4}) + 0.4 \quad . \tag{45}$$

The data $\tilde{g}$ and $\tilde{f}$ are given by (42) and (43). The Dirichlet condition on $\partial\tilde{\mathcal{D}}$ is homogeneous. Assume that the data of the discrete problem g and f are exactly $\tilde{g}$ and $\tilde{f}$. As the L-scheme, with a Neumann condition, is a first order method, $\tilde{\psi}$ is perturbed at the order 1 with

$$\psi = \tilde{\psi} + 0.01 \sin\left(\frac{3\,x}{h}\right) \cos\left(\frac{2\,y}{h}\right) h, \quad \text{in } \mathcal{D}.$$

Note that the factor 0.01 is applied to avoid a too excessive amplitude of the first order oscillations. For the Q-scheme and the C-scheme, a second order perturbation on $\tilde{\psi}$ is tested. The normal vector, given by the gradient of the level set function, should also be at the order 2 at least, so that the boundary condition is second order accurate. Set

$$\psi = \tilde{\psi} + \cos(\pi\, x\, y)\; h^2 + \sin\left(\frac{3\,x}{h^2}\right) \cos\left(\frac{2\,y}{h^2}\right) h^4, \quad \text{in } \mathcal{D}.$$

Table 18 and Figure 20 show the results of the numerical accuracy tests.

Number of points	u L^∞-error	order	$\nabla^h u$ L^∞-error	order	$\nabla \cdot \nabla^h u$ L^∞-error	order
96	1.651×10^{-3}	-	4.606×10^{-2}	-	3.344×10^{0}	-
144	1.103×10^{-3}	0.99	3.039×10^{-2}	1.03	3.235×10^{0}	0.08
216	7.160×10^{-4}	1.03	2.019×10^{-2}	1.02	2.971×10^{0}	0.15
324	3.932×10^{-4}	1.18	1.393×10^{-2}	0.98	2.951×10^{0}	0.10
96	2.145×10^{-4}	-	6.009×10^{-3}	-	9.900×10^{-1}	-
144	9.712×10^{-5}	1.95	3.186×10^{-3}	1.57	7.042×10^{-1}	0.84
216	5.079×10^{-5}	1.78	1.364×10^{-3}	1.83	5.169×10^{-1}	0.80
324	2.082×10^{-5}	1.92	6.747×10^{-4}	1.80	3.123×10^{-1}	0.95
96	7.103×10^{-5}	-	2.044×10^{-3}	-	3.304×10^{-1}	-
144	2.999×10^{-5}	2.13	1.009×10^{-3}	1.74	1.627×10^{-1}	1.75
216	1.620×10^{-5}	1.82	4.716×10^{-4}	1.81	8.160×10^{-2}	1.72
324	6.872×10^{-6}	1.92	2.051×10^{-4}	1.89	3.415×10^{-2}	1.87

Table 18: L-scheme (top), Q-scheme (middle) and C-scheme (bottom) with a perturbed interface for the Neumann problem of Test-case 13.

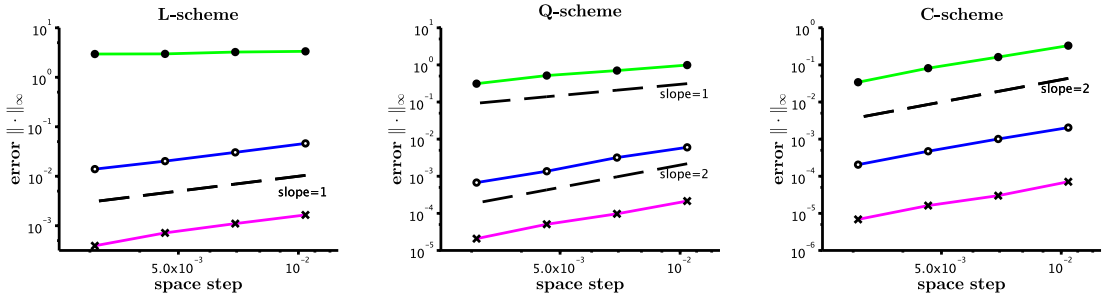

Figure 20: Numerical results for the Neumann problem of Test-case 13 with a perturbed interface.

Note that the optimality of the interface perturbation for the Q-scheme is not absolutely clear. Disrupting the interface at the order 2 with a first order accuracy on the gradient of the level set, for different geometries and data, leads to quasi-superconvergence –see Figure 21 These results are summarized in Table 19.

4.3 Application to the dynamical coupled problem of invadopodia

The purpose is to show that our superconvergent methods generate better convergence rates of the solution, in the context of a strongly coupled dynamic problem. Invadopodia are localized finger-like projections that grow at the cytoplasmic membrane of pre-metastatic cancer cells. This active change in morphology enables them to invade nearby tissues and to migrate through the body to create secondary tumor foci, called metastasis. The interested reader can refer to [7] for details about the biological phenomenon of invadopodia and the choice of the model. It can

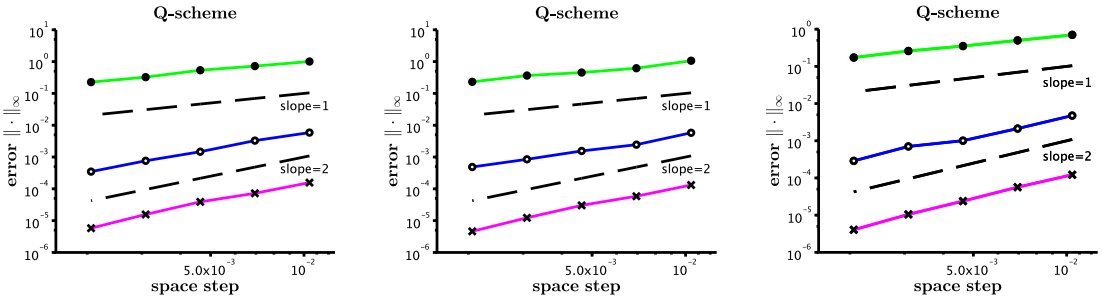

Figure 21: Quasi-superconvergence of the Q-scheme with a first order accurate normal vector. Left: $\tilde{\Gamma}$ is defined by (45). Middle: $\tilde{\Gamma}$ is a circle. Right: $\tilde{\Gamma}$ is an ellipse (Test-case 13).

	level set accuracy		solution accuracy		
	ψ	$\nabla^h\psi$	u	$\nabla^h u$	$\nabla^h\cdot\nabla^h u$
L-scheme	1		1	1	0
Q-scheme	2	2 (1?)	2	2	1
C-scheme	2	2	2	2	2

Table 19: Order of accuracy of the interface location (left) required to obtain superconvergence properties (right) for a Neumann problem, with respect to the considered numerical scheme. The requirement on $\nabla^h\psi$ for the Q-scheme is not clear.

be summarized as follows: consider the problem (35)-(39), with $\tilde{f}_1 = \tilde{f}_2 = 0$, and define the interface velocity by

$$\tilde{\mathbf{v}} = \nabla\tilde{u}_2, \quad \text{in } \tilde{\Omega}_2.$$

Consider $\tilde{\mathbf{w}}$ an extension of $\tilde{\mathbf{v}}$ in $\tilde{\mathcal{D}}$. The interface is then advected using

$$\partial_t\tilde{\psi} + \tilde{\mathbf{w}}\cdot\nabla\tilde{\psi} = 0, \quad \text{in } \tilde{\mathcal{D}}. \tag{46}$$

In [7], the problem is numerically solved using the simplest second order methods for the static part of the problem: the Q-scheme for the Neumann problem and the L-scheme for the Dirichlet problem. The velocity is extended at the order 1 and equation (46) is discretized with the usual forward Euler method for the time derivative and the WENO5 scheme for the flux. $\tilde{\psi}$ is the main unknown of the coupled problem since it gives the shape of the tumor cell at each numerical time. The numerical accuracy tests highlight the first order accuracy of the solution. In our study, as the purpose is to achieve a better accuracy of the solution, the forward Euler method is replaced by the RK2 method and the extended velocity is computed with a second order method of extension, based on the same principle as in [7]. We do not give the details of these methods, since we are mainly interested in the influence of the superconvergent schemes –that are used for the static part of the problem– on the solution at the final time. We just specify that the method of velocity extension preserves the second order of accuracy of the extended velocity and its divergence. To ensure that the velocity extension and the transport do not impact the first order accurate results in [7], we first perform the simulation with the Q and L-schemes. We then use alternatly Q-schemes and C-schemes for both Neumann and Dirichlet problems. At the initial time, $\tilde{\Gamma}_0$ is defined by $\tilde{\psi}_0$ as the circle of center $(0,0)$ and radius 0.3. At each numerical

time, the boundary data is given as the trace of

$$\forall (r,\theta) \in \tilde{\Gamma}_t, \quad G(r,\theta) = \begin{cases} 0.05 + 3\,\exp\left(\dfrac{0.1}{(\theta + \frac{10\,\pi}{15})\,(\theta + \frac{8\,\pi}{15})}\right) & \text{if } \frac{-10\,\pi}{15} < \theta < \frac{-8\,\pi}{15}, \\ 0.05 + 2\,\exp\left(\dfrac{0.1}{(\theta + \frac{7\,\pi}{15})\,(\theta + \frac{5\,\pi}{15})}\right) & \text{if } \frac{-7\,\pi}{15} < \theta < \frac{-5\,\pi}{15}, \\ 0.05 & \text{otherwise.} \end{cases} \tag{47}$$

The simulation is performed until the final time $T = 0.3$. The reference solution is computed on a 1000×1000 grid, for 376 iterations. Errors on ψ and $\mathbf{n}$ are computed on a small tubular area around the interface $\tilde{\Gamma}$, in order to avoid the ridges that are generated by the velocity extension. Table 20 and Figure 22 show the results of the numerical accuracy tests for the level set function and the normal vector.

schemes	Number of points	Number of iterations	ψ L^∞-error	order	$\mathbf{n}$ L^∞-error	order
Q-L	96		2.552×10^{-3}	-	1.533×10^{-1}	-
	144		1.495×10^{-3}	1.32	1.007×10^{-1}	1.03
	216		1.080×10^{-3}	1.06	8.426×10^{-2}	0.74
	324		6.833×10^{-4}	1.08	5.589×10^{-2}	0.83
	486		4.300×10^{-4}	1.10	3.772×10^{-2}	0.86
Q-Q	96		7.378×10^{-4}	-	8.486×10^{-2}	-
	144		2.860×10^{-4}	2.34	4.062×10^{-2}	1.82
	216		1.284×10^{-4}	2.16	2.580×10^{-2}	1.47
	324		6.583×10^{-5}	1.99	1.370×10^{-2}	1.50
	486		3.224×10^{-5}	1.93	6.703×10^{-3}	1.57
C-C	96		5.410×10^{-4}	-	5.374×10^{-2}	-
	144		1.774×10^{-4}	2.75	3.556×10^{-2}	1.02
	216		1.051×10^{-4}	2.02	1.522×10^{-2}	1.56
	324		3.205×10^{-5}	2.32	6.785×10^{-3}	1.70
	486		1.132×10^{-5}	2.38	2.574×10^{-3}	1.87

Table 20: Numerical results of accuracy for the simulation of invadopodia, with respect to the numerical schemes used for the static part of the problem.

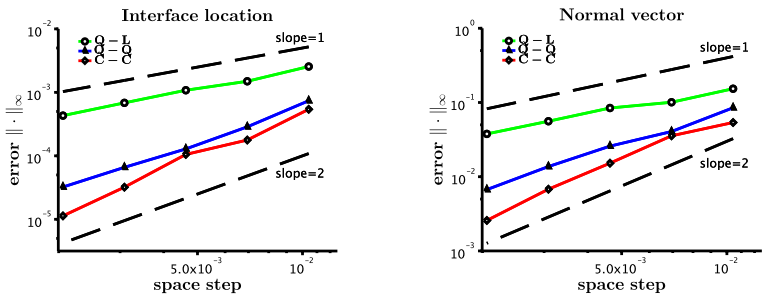

Figure 22: Numerical results of accuracy on the interface location (left) and the normal vector (right) for the simulation of invadopodia, with respect to the schemes used for the static part of the problem.

Results confirm the first order accuracy on the interface location and the normal vector for the Q-L scheme combination, as highlighted in [7]. The Q-Q combination gives an accuracy at order 2 for the interface location and approximately at the order 1.5 for the normal vector. Finally, the C-C combination is fully second order accurate, with a slightly better accuracy on the interface location than with the Q-Q combination.

5 Conclusion

We have proposed superconvergent Cartesian methods to solve the Poisson equation on domains, with a Dirichlet, a Neumann or a Robin condition on the boundary of the domain. These methods are based on the Ghost Fluid Method and linear, quadratic or cubic extrapolations of the ghost values. Throughout several test-cases on 2D-domains, we have classified the superconvergence properties, with respect to the considered scheme. We have also identified some required criteria of accuracy on the boundary data and the interface location to achieve superconvergence: surprisingly, the data do not have to be high-order accurate but just require to be superconvergent themselves. It is worth noting that those criteria imply that the Laplace operator is zeroth order accurate near the interface. Nevertheless, we are able to obtain a second order accuracy of the solution and its first and second derivatives in the case of cubic extrapolations. Note also that, although it is not equivalent to perturb the one or the other (when the distances to the interface are not exactly known), the criteria on the boundary data and on the interface location seem to be similar. The superconvergence results and criteria on data are all summarized in the final table 21. If superconvergence has already been studied and proved in other works, in the case of exact data, the transmission of the superconvergence properties, from second order superconvergent data to the solution, are still an open issue. We are confident that this study is a step towards the theoretical understanding of this transmission phenomenon. The transmission of superconvergence properties is one of the main results of the paper. This makes it possible to solve some coupled problem and obtain better convergence rates. Or even to avoid losing the consistency of the solution, if an unknown depends on the first or second derivative of another. In particular, our methods are well suited to free boundary problems, in which the interface location may be an approximate at each numerical time. Obviously, these methods use wide stencils. The parallel implementation of the code –for a three-dimensional use for instance– is somewhat more complex to carry out, requiring three communication layers, at worst. However, they are a real benefit to get superconvergence properties and solve coupled problems.

	Dirichlet			**Neumann**		
	L-scheme	Q-scheme	C-scheme	L-scheme	Q-scheme	C-scheme
Order of accuracy required on data						
g	2	2	2	1	2	2
$\partial^h_\tau g$		2	2			2
$\partial^h_{\tau\tau} g$			2			
ψ	2	2	2	1	2	2
$\nabla^h \psi$		2	2		2 (1?)	2
$\nabla^h \cdot \nabla^h \psi$			2			
Order of accuracy of the solution						
u	2	2	2	1	2	2
$\nabla^h u$	1	2	2	1	2	2
$\nabla^h \cdot \nabla^h u$	0	1	2	0	1	2

Table 21: Zoology of the Cartesian numerical methods to solve the Poisson equation, and their superconvergence properties, with minimal requirements on data accuracy.

Acknowledgements

This study has been supported by the French National Research Agency (ANR) in the frame of the "Investments for the future" Programme IdEx Bordeaux - CPU (ANR-10-IDEX-03-02) and by the Core program Advanced Research Networks, granted by the JSPS Core.

Numerical simulations presented in this paper were carried out using the PLAFRIM experimental testbed, being developed under the Inria PlaFRIM development action with support from LABRI and IMB and other entities: Conseil Régional d'Aquitaine, FeDER, Université de Bordeaux and CNRS (see https://plafrim.bordeaux.inria.fr/).

References

[1] Ivo Babuška, Uday Banerjee, and John E. Osborn. Superconvergence in the generalized finite element method. *Numerische Mathematik*, 107(3):353–395, 2007.

[2] Han Chen, Chohong Min, and Frédéric Gibou. A Supra-Convergent Finite Difference Scheme for the Poisson and Heat Equations on Irregular Domains and Non-Graded Adaptive Cartesian Grids. *Journal of Scientific Computing*, 31(1–2):19–60, 2007.

[3] Philippe G. Ciarlet. Discrete maximum principle for finite-difference operators. *aequationes mathematicae*, 4(3):338–352, 1970.

[4] Marco Cisternino and Lisl Weynans. A parallel second order Cartesian method for elliptic interface problems. *Communications in Computational Physics*, 12:1562–1587, June 2012.

[5] Ronald P. Fedkiw, Tariq Aslam, Barry Merriman, and Stanley Osher. A Non-oscillatory Eulerian Approach to Interfaces in Multimaterial Flows (the Ghost Fluid Method). *Journal of Computational Physics*, 152(2):457–492, 1999.

[6] José A. Ferreira and Rolf D. Grigorieff. On the supraconvergence of elliptic finite difference schemes. *Applied Numerical Mathematics*, 28(2–4):275 – 292, 1998.

[7] Olivier Gallinato, Masahito Ohta, Clair Poignard, and Takashi Suzuki. Free boundary problem for cell protrusion formations: theoretical and numerical aspects. Research Report 8810, INRIA; Université de Bordeaux; Tokyo University of Science; Osaka University. 2015, pp.35. hal-01228013.

[8] Frederic Gibou, Ronald P. Fedkiw, Li-Tien Cheng, and Myungjoo Kang. A Second-Order-Accurate Symmetric Discretization of the Poisson Equation on Irregular Domains. *Journal of Computational Physics*, 176:205–227, 2002.

[9] Nick Levine. Superconvergent Recovery of the Gradient from Piecewise Linear Finite-element Approximations. *IMA Journal of Numerical Analysis*, 5(4):407–427, 1985.

[10] Zi-Cai Li, Tetsuro Yamamoto, and Qing Fang. Superconvergence of solution derivatives for the Shortley–Weller difference approximation of Poisson's equation. part I: smoothness problems. *Journal of Computational and Applied Mathematics*, 151(2):307–333, 2003.

[11] Nami Matsunaga and Tetsuro Yamamoto. Superconvergence of the Shortley–Weller approximation for Dirichlet problems. *Journal of Computational and Applied Mathematics*, 116(2):263–273, 2000.

[12] Chohong Min, Frédéric Gibou, and Hector D. Ceniceros. A supra-convergent finite difference scheme for the variable coefficient Poisson equation on non-graded grids. *Journal of Computational Physics*, 218(1):123–140, 2006.

[13] George H. Shortley and Royal Weller. The Numerical Solution of Laplace's Equation. *Journal of Applied Physics*, 9(5):334, 1938.

[14] Lisl Weynans. A proof in the finite-difference spirit of the superconvergence of the gradient for the Shortley-Weller method. Research Report, RR-8757, INRIA Bordeaux; INRIA. 2015, pp.14. hal-01176994.

[15] Gangjoon Yoon and Chohong Min. Convergence Analysis of the Standard Central Finite Difference Method for Poisson Equation. *Journal of Scientific Computing*, pages 1–16, 2015.

[16] Milŏs Zlámal. Superconvergence and reduced integration in the finite element method. *Mathematics of Computation*, 32(143):663–685, 1978.

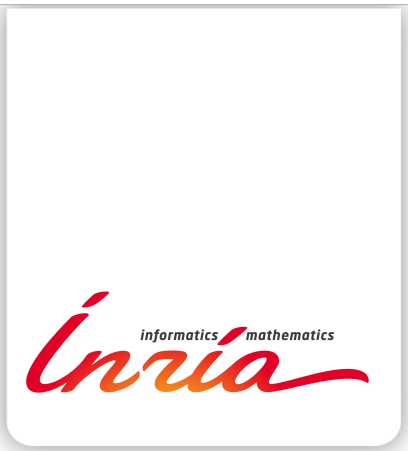

RESEARCH CENTRE
BORDEAUX – SUD-OUEST

200 avenue de la Vieille Tour
33405 Talence Cedex

Publisher
Inria
Domaine de Voluceau - Rocquencourt
BP 105 - 78153 Le Chesnay Cedex
inria.fr

ISSN 0249-6399